NTNU

Norwegian University of
Science and Technology

A comparative Analysis of Propane and Ethylene Glycol as Intermediate Fluid in a LNG Regasification System

Erik Langaard Solberg

Master of Science in Mechanical Engineering
Submission date: August 2015
Supervisor: Trygve Magne Eikevik, EPT
Co-supervisor: Wensheng Lin, Shanghai Jiao Tong University

Norwegian University of Science and Technology
Department of Energy and Process Engineering

Norwegian University of Science and Technology
Faculty of Engineering Science and Technology
Department of Energy and Process Engineering

EPT-P-2015-86

NTNU

MASTER THESIS

for

student Erik Langaard Solberg

Spring 2015

A comparative analysis of propane and ethylene glycol as intermediate fluid in a LNG regasification system

En sammenlignende studie av propan og etylenglykol som mellommedium i en LNG-terminal

Background and objective

LNG in China is a relatively new energy source, though a rapidly increasing one. China imports LNG to account for the increasing gas demand and the annual consumption will reach an estimated 200 billion cubic metres by 2020. The first LNG regasification terminal in China, the Shenzhen Dapeng terminal, was operational in 2006 with a capacity of 3.7 Mtpa. More terminals are currently being planned, built or expanded.

The work will focus on a LNG regasification system with an intermediate fluid vaporizer. The work is to compare propane and a mixture of water and ethylene glycol as the intermediate fluid and investigate the fluids' heat transfer properties. The regasification should be aimed at the Chinese gas network and Chinese demands. The LNG-intermediate fluid heat exchange is to be simulated using ANSYS Fluent and validated by comparison to empirical measurements.

The work is part of a research group at the Shanghai Jiao Tong Uni. funded by the Ministry of Industry and Information Technology of China.

The following tasks are to be considered:

1. Literature review of LNG heat exchange and regasification systems.
2. Specify the foundation and conditions on which simulations and experiments are carried out.
3. Simulate heat exchange using software from Ansys and conduct empirical experiments.
4. Compare simulations and experiment results and discuss deviations, if any.
5. Compare the different intermediate fluids and assess their value as heat transfer agent.
6. Conclude
7. Make a proposal of further work

-- " --

The master thesis work comprises 30 ECTS credits.

The work shall be edited as a scientific report, including a table of contents, a summary in Norwegian, conclusion, an index of literature etc. When writing the report, the candidate must emphasise a clearly arranged and well-written text. To facilitate the reading of the report, it is important that references for corresponding text, tables and figures are clearly stated both places.
By the evaluation of the work the following will be greatly emphasised: The results should be thoroughly treated, presented in clearly arranged tables and/or graphics and discussed in detail.

The candidate is responsible for keeping contact with the subject teacher and teaching supervisors.

Risk assessment of the candidate's work shall be carried out according to the department's procedures. The risk assessment must be documented and included as part of the final report. Events related to the candidate's work adversely affecting the health, safety or security, must be documented and included as part of the final report. If the documentation on risk assessment represents a large number of pages, the full version is to be submitted electronically to the supervisor and an excerpt is included in the report.

According to "Utfyllende regler til studieforskriften for teknologistudiet/sivilingeniørstudiet ved NTNU" § 20, the Department of Energy and Process Engineering reserves all rights to use the results and data for lectures, research and future publications.

The report shall be submitted to the department in 3 complete, bound copies.

An executive summary of the thesis including title, student's name, supervisor's name, year, department name, and NTNU's logo and name, shall be submitted to the department as a separate pdf file. The final report in Word and PDF format, scientific paper and all other material and documents should be given to the academic supervisor in digital format on a DVD/CD-rom or a memory stick at the time of delivery of the project report.

Submission deadline: *August 25, 2015.*

☐ Work to be done in lab (Water power lab, Fluids engineering lab, Thermal engineering lab)

☐ Field work

Department for Energy and Process Engineering, 22 August 2014.

Prof. Olav Bolland	Prof Trygve M. Eikevik
Department Head	Academic Supervisor

Supervisors:

Prof. Lin Wensheng, Shanghai Jiao Tong University, linwsh@sjtu.edu.cn

Prof Trygve M. Eikevik, NTNU, trygve.m.eikevik@ntnu.no

Preface

This master thesis studies two heat transfer fluids, propane and a mixture of mono-ethylene glycol and water, in a LNG regasification system with an intermediate fluid vaporizer. The mixture contains 50 mass% mono-ethylene glycol and is henceforth referred to only as “glycol”. The fluids are studied through simulations using the computational fluid dynamics (CFD) software package Ansys FLUENT. A suitable experiment is designed and conducted to verify the simulations, as well as gain practical knowledge of the heat transfer processes. The two fluids are compared and their use in industrial scale plants is discussed.

The work is conducted at the Shanghai Jiao Tong University (SJTU) and is supervised by Professor Lin Wensheng and Professor Trygve Magne Eikevik (Norwegian University of Science and Technology, NTNU). I would like to express my sincere gratitude to the Chinese employees and students at STJU: firstly Master Liu Huaxuan (刘华萱) who, despite only speaking Chinese, provided invaluable help and hands-on laboratory knowledge. Furthermore I could not have completed the work without help with laboratory work and translations from Dr. Wang Gang (王刚) og Dr. Zhang Hua (张华).

Erik Langaard Solberg

Oslo, July 2nd 2015

Nomenclature

LNG		Liquefied Natural Gas
IF		Intermediate Fluid
Glycol		50 mass-% mixture of mono-ethylene glycol and water
bcm	bcm	Billion cubic meters
Q	kW	Heat
m	kg/s	Mass flow
c_p	kJ/kgK	Heat capacity
T	K or ℃	Temperature
U	W/m^2K	Overall heat transfer coefficient
A	m^2	Heat transfer surface area
ΔT_{LM}	K	Logarithmic mean temperature difference
LMTD	K	Logarithmic mean temperature difference
h	W/m^2K	Film heat transfer coefficient
R	m^2K/W	Fouling resistance
Δx_w	m	Wall thickness
k	W/mK	Thermal conductivity
Nu_L	dimensionless	Nusselt number
L	m	Characteristic length
Tpd	tpd	Tonnes per day
MTPA	MTPA	Million tonnes per annum
ρ	kg/m^3	density
P	bar, kPa or MPa	pressure
t	s	time
U		Flow velocity vector field
∇		Del operator
τ		Total stress tensor
g		Body forces per unit volume
k		Turbulent kinetic energy
ε		Turbulence dissipation rate
ω		Specific dissipation rate

Summary

A LNG regasification system with intermediate fluid vaporizer is studied. Two different intermediate fluids (IF), propane and a mix of mono-ethylene glycol and water, are compared for use in the system. The regasification system consists of two tube-in-tube heat exchangers, where the IFs flow between the two. Liquid nitrogen (used instead of LNG for safety and practicality) is evaporated and heated in the cold side heat exchanger by the IF, while water heats the IF in the second, warm side heat exchanger. Neither IF change phase during the loop.

The work presented is conducted at the Shanghai Jiao Tong University in China. A small-scale rig is built in the campus laboratory and experiments are conducted with the two IFs. Simultaneously computer simulations with Ansys FLUENT are verified by the experiments. The thesis presents a relevant background for LNG terminals and import in China and explains the fundamental mathematics used by the simulation software. The simulation, including building geometry and mesh grids, conducting independence studies, setting up the simulation case and boundary conditions, solving and reaching convergence are thoroughly explained. The experiment build and performance is outlined as well, and is further detailed in the appendices.

The simulations, when verified by experiments, are used to compare propane and glycol as heat transfer fluids under exactly equal conditions. The comparison is discussed in relation to industrial-scale regasification plants and some recent scientific papers. The restrictions and differences of the IFs impact the use in different cases. Furthermore the overall regasification system is subject to discussion as well. It is found that more research is needed to further develop the overall system.

Sammendrag

Fokus for denne masteroppgaven er et LNG regassifiseringssystem med mellomfluid. Mellomfluidet fører varme fra varmekilden, sjøvann, til LNG, som varmes opp og blir til gass klar til bruk. I denne oppgaven studeres propan og en blanding av 50 masse-% glykol og vann som mellomfluid. Stoffenes egenskaper som mellomfluider studeres og sammenlignes. Regassifiseringssystemet består av to rørvarmevekslere, der mellomfluidet trekker varme fra vann i den ene og tilfører varme til LNG i den andre. Det er ingen faseendring på mellomfluidene. I denne oppgaven brukes nitrogen istedenfor LNG for å gjennomføre sikkert arbeid.

Det presenterte arbeidet er utført ved Shanghai Jiao Tong-universitetet i Kina. Systemet undersøkes ved hjelp av forsøk og simuleringer med Ansys FLUENT. Et regassifiseringssystem i laboratorieskala er bygget på campus. Denne masteroppgaven presenterer en relevant bakgrunn for LNG-terminaler og –import i Kina, samt relevant matematikk som ligger til grunn for forsøk og simuleringer. Både simulering og forsøk er grundig forklart. Forsøk og simuleringer er utført for like forhold og resultatene presenteres og diskuteres i de siste kapitlene av oppgaven. Detaljer for forsøkene er å finne som vedlegg.

Simuleringene er verifisert av forsøk. Deretter sammenlignes glykol-blandingen og propan i tjeneste som varmemedier i systemet. Sammenligningen diskuteres i forhold til industriskala LNG-terminaler og nylig forskning. I enkelte, forskjellige tilfeller har fluidene begrensninger som kan gjøre dem uegnede for bruk i regassifiseringssystemer. Dette medfører at de to fluidene dekker noe forskjellige bruksområder. Videre diskuteres systemet som helhet. Dette spesifikke systemet trenger videre utvikling før det kan settes i kommersiell bruk.

Table of contents

1.0 Introduction

LNG as an energy resource is experiencing increasing importance across the world in general, and in China in particular. Among the fossil fuels natural gas is the cleanest-burning source of energy and is vital for China to sustain its still rapidly growing economy. China is aiming to move from a significant coal dependency to greener sources of energy. According to estimates (Wang et. al., 2006) China's consumption of natural gas will increase from 100 bcm (billion cubic metres) to 200 bcm from 2010 to 2020, though China's own production will only reach 120 bcm in 2020. Some natural gas is imported through pipelines from Russia and the central Asian countries, but a significant amount will also reach the Chinese mainland as LNG. Thus there is high need for LNG receiving terminals, in which the regasification system is central.

On a global scale transport of natural gas as LNG is increasing. According to BP's annual statistical review of world energy (2014), LNG's share in global gas trade is 31.4%. The trend in the USA is generally moving from importing to exporting with the increased production of shale gas, driving prices down in the American region, as illustrated in figure 1. Receiving terminals are converted to exporting terminals. Furthermore LNG production in Australia is increasing, with 4 LNG plants in operation and 6 in construction. The prices in the Asian region are still high, making it a logical target for export.

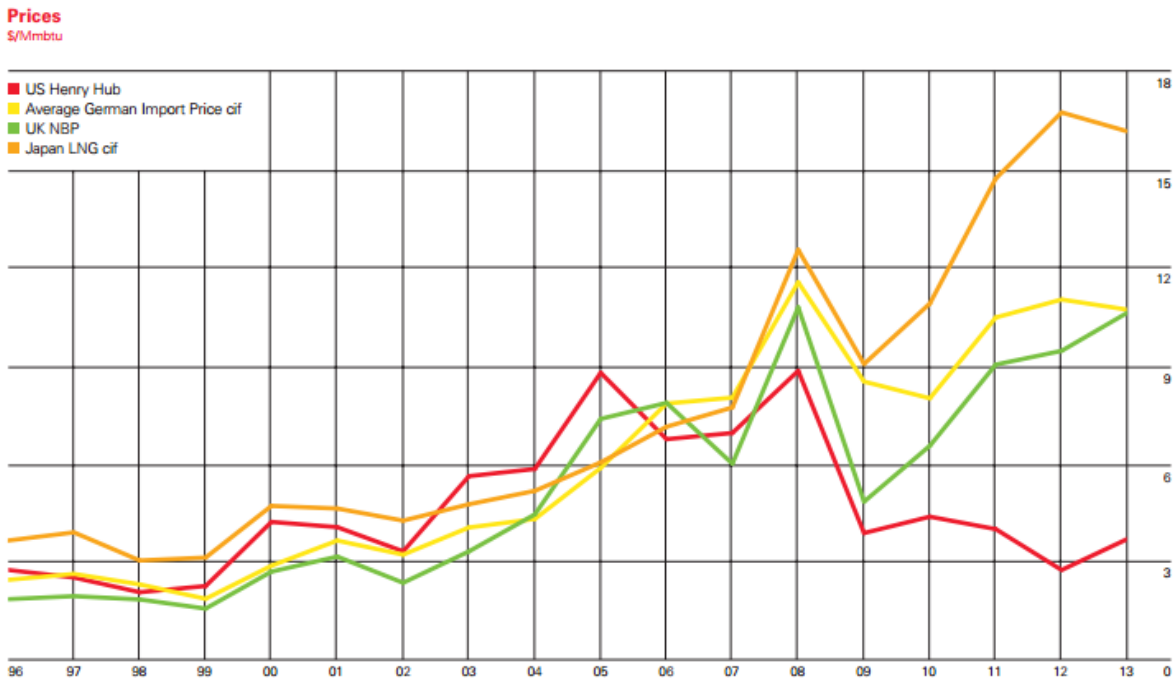

Figure 1: Gas prices of 2014, BP review of world energy

As illustrated by figure 2, gas imports in China are increasing. China was in 2012 the third largest importer of LNG, only surpassed by Japan and South Korea, and LNG imports measured 24.3 bcm in 2013 (US. Energy Information Administration, 2014).

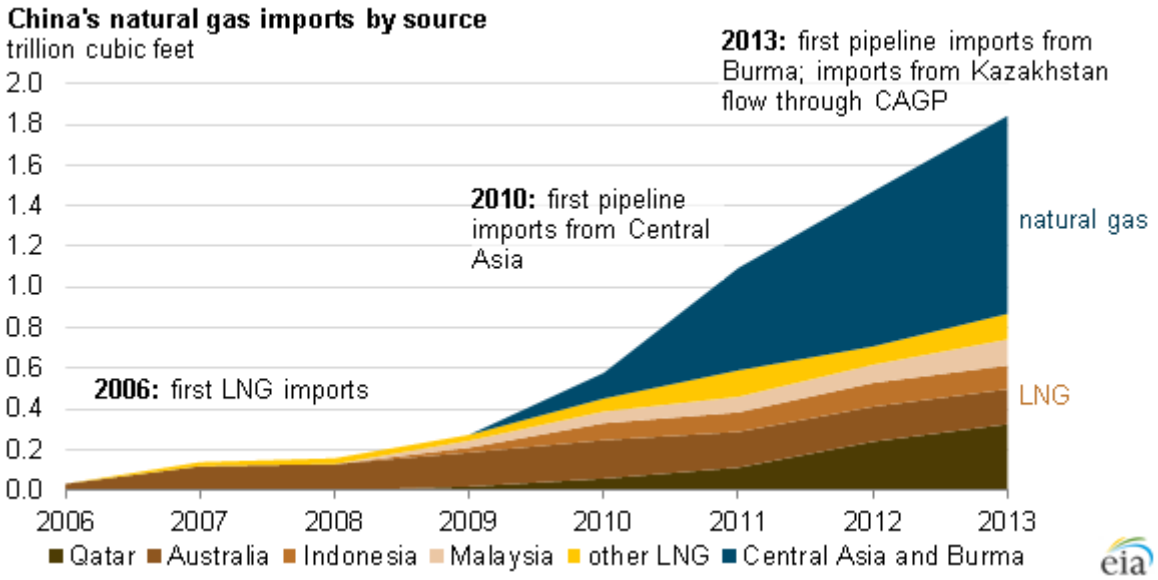

Figure 2: China's natural gas imports by source

China continues to invest in both LNG terminals, LNG infrastructure and conventional pipeline infrastructure. The country will import gas by pipeline from Russia, Myanmar, Turkmenistan and Kazakhstan, among others. There are as of 2014 10 major LNG regasification terminals in China (US. Energy Information Administration, 2014), with several ongoing or planned expansion and new construction projects. The Shenzhen Dapeng LNG terminal, the first in China, was operational in 2006. Figure 3 lists the current and proposed major Chinese LNG terminals (US. Energy Information Administration, 2014)

Terminal name	Status/online date	Developer	Capacity – init./exp. (MMcf/d)	Possible supplier
Wuhaogou Dapeng/Guangdong	Operational; Second Expansion - 2014	CNOOC; BP	885 / 530	Australia NWS
Peaking Facility	Operational	Shanghai Gas Group	15	Spot cargoes
Fujian	Operational	CNOOC; Fujian Investment Co.	345	Indonesia - Tangguh
Shanghai	Operational; Expansion - 2015	CNOOC; Shenergy Group	395 / 395	Malaysia - Petronas

Terminal name	Status/online date	Developer	Capacity – init./exp. (MMcf/d)	Possible supplier
Dalian	Operational; Expansion - 2015	CNPC	395 / 395	QatarGas IV; Australia
Rudong/Jiangsu	Operational; Expansion(Permitting) / 2014	CNPC; RGM; CITIC	460 / 395	QatarGas IV
Zhejiang/Ningbo	Operational	CNOOC	395	QatarGas III
Zhuhai	Operational; Expansion / 2017	CNOOC	460 / 460	Not determined
Tianjin FSRU	Operational; Onshore terminal expansion proposed	CNOOC	290 / 795	Not determined
Caofeidian/Tangshan	Operational	CNPC	460	Australia and Qatar
Qingdao/ Shandong	Construction / 2014; Expansion	Sinopec; Huaneng Group	395 / 265	PNG LNG (ExxonMobil) and APLNG
Hainan	Construction / 2014; Expansion / 2017	CNOOC; Hainan Development	260 / 130	Not determined
Beihai/Guangxi	Construction / 2014; Expansion / 2020	Sinopec	395 / 395	Papua New Guinea LNG and Australia Pacific LNG
Shenzhen/Diefu	Construction / 2015	CNOOC; Shenzhen Energy	530	Not determined
Tianjin	Construction / 2016	Sinopec	395	Australia Pacific LNG
Shantou	Awaiting NDRC approval / 2014 (Phase 1) and 2017 (Phase 2)	SinoGas	160 / 240	Australia
Jiangsu/Yancheng FSRU	Planning; NEA approval received August 2013 / 2014	CNOOC	290	Not determined
Yantai, Shandong FSRU	Planning / 2013	CNOOC	200	Not determined
Shenzhen	NDRC approval; Awaiting siting permit / 2015	CNPC; CLP	400	Australia's Gorgon LNG (ExxonMobil)
Yuedong/Jieyang	Environmental approval; Awaiting NDRC approval / 2014 / Expansion in 2020	CNOOC	260 / 260	Not determine

Figure 3: China's major LNG terminals

2.0 Literature survey

A regasification plant as part of a LNG terminal vaporizes LNG to gas at ambient temperature. It is then usually sent to a gas pipeline, or transported by other means as CNG, to consumers. The plants can be placed on land or floating barges; floating barges have the advantage of being able to move to new locations if the business environment changes.

Most LNG plants are located close to seawater as LNG is frequently transported by ship. Therefore the conventional regasification plant draws heat from seawater to gasify the LNG. Seawater is preferable to other, more costly sources of heat. The main opposition is environmental concerns towards impact on marine life due to high cold water discharge and chemical residuals. Several different technologies exist as alternatives.

2.1 Regasification plant vaporizers

The vaporizer or evaporator is the central part of any regasification plant. Traditionally the most common technology is the open rack vaporizer, which accounts for about 70% of installed units. Submerged combustion vaporizers account for about 25%, whereas intermediate fluid vaporizers have been used for a few systems. Direct air vaporizers and ambient air vaporizers are known to be used in smaller plants and peak shaving facilities (Patel et. al., 2013).

Open Rack Vaporizer (ORV)

The Open Rack Vaporizer is a widely used regasification technology that exchanges heat with seawater, preferably above 5℃. They are typically constructed in an aluminium alloy to tolerate cryogenic conditions and to have a high heat transfer coefficient. The layout is shown in figure 4. LNG flows from the bottom through a pipe panel and leave as gas at the top. Seawater flows downwards on the outside of the panel, which is coated with a corrosive-resistant layer. ORVs must be regularly maintained to keep the surface clean and free of ice.

ORVs require a large amount of water, which must be filtrated for sand or other fouling particles, and be free of heavy metal ions that may damage the anti-corrosive coating. Environmental considerations must be made; the seawater temperature drop is generally limited to 5℃ to avoid impact on the marine habitat.

Fuel Gas heating (FG)

Fuel gas heating, as the name implies, involves heating LNG with fuel gas. The gas is typically 1.5% of the vaporized LNG, which decreases the output and revenue of the plant. This type of heating is usually supplied by a SCV (described below) to an ORV in peak months or in winter if the seawater

temperature is too low. The burners can be designed to burn both low-pressure boil-off gas from storage tanks or product gas from the regasification system.

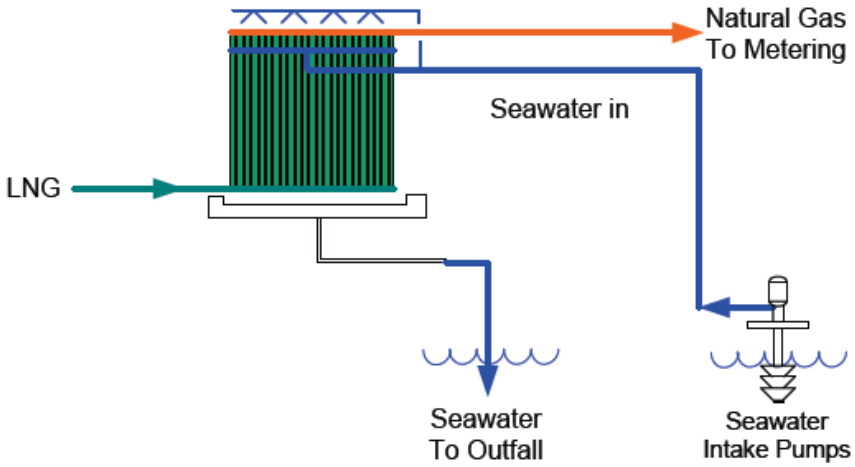

Figure 4: Open-rack vaporizer

Submerged Combustion Vaporizer (SCV)

In a submerged combustion vaporizer the LNG flows through a tube submerged in a water bath. The water bath is heated by flue gas from a combustion process. The process is shown in figure 5. The flue gas is distributed evenly throughout the bath, with turbulence-promoting distributors. Turbulence increases the rate of heat transfer and reduces scaling or fouling of the heat transfer surface.

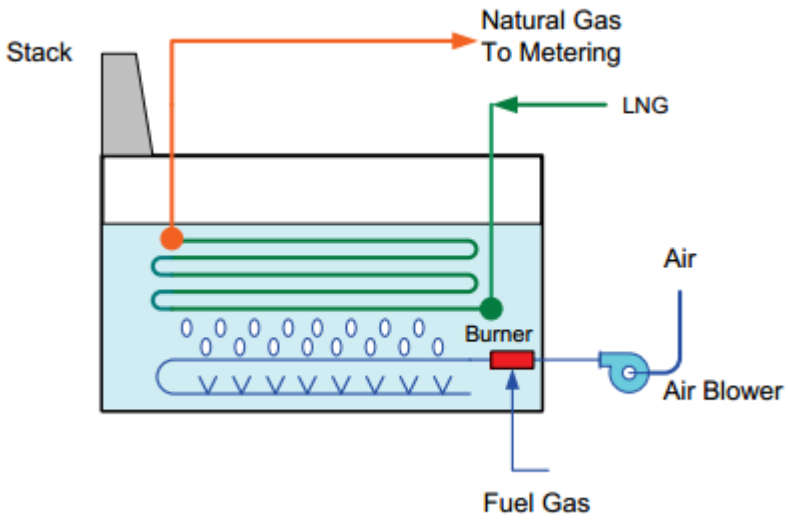

Figure 5: Submerged combustion vaporizer

The pH-levels of the SCV water bath must be controlled, as the CO_2 from the combustion will condense and acidify the water, which may cause corrosion. Caustic chemicals such as sodium carbonate and sodium bicarbonate are common additives to control the pH-levels. The burners are subject to normal industrial specifications with regard to NO_x and other emissions. A SCV requires less space than an ORV, though it requires more equipment.

Ambient Air Vaporizer (AAV)

These vaporizers are high vertical heat exchangers, considerable larger than ORVs. For this reason they are mainly used in peak shaving plants and smaller terminals. The AAV configuration is shown in figure 6.

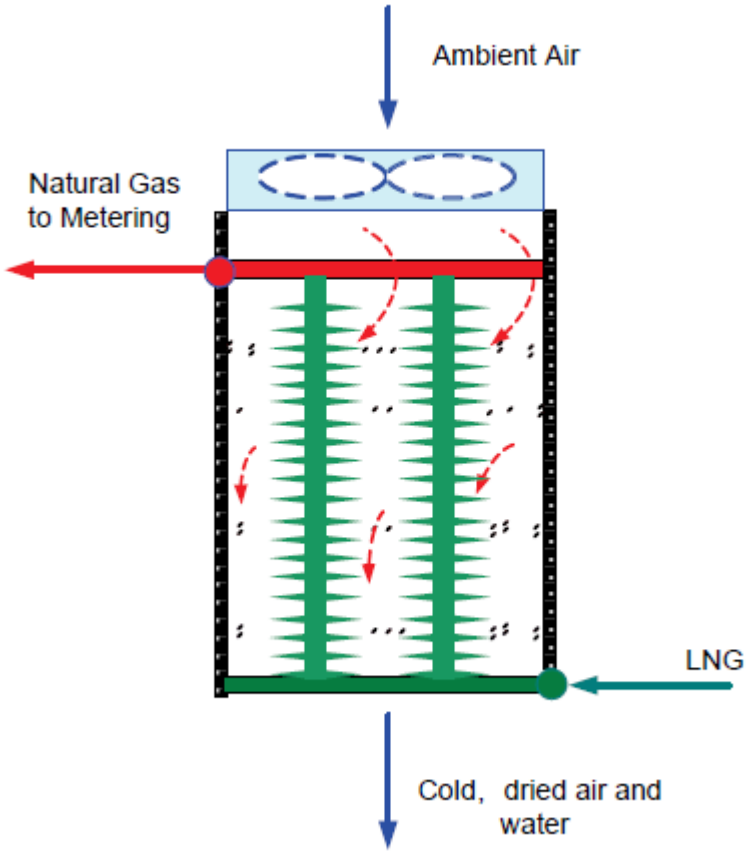

Figure 6: Ambient Air Vaporizer

AAVs feature a downward stream of ambient air due to the lower density of the cold air as it exchanges heat with the LNG. The air draft may be natural or forced. Due to water condensation and freezing on the heat exchanger racks they require frequent defrosting, typically within a 4-8 hour cycle. AAVs depend greatly on environmental factors, such as ambient temperature, solar radiation, wind and humidity. Naturally they operate better in warm climates than cold.

Intermediate Fluid Vaporizers (IFV)

Intermediate fluid vaporizers use an intermediate fluid (IF) to vaporize the LNG. The intermediate fluid flows in a closed loop and draws heat form a secondary source, such as seawater or an industrial process. There are three types of intermediate fluid typically used for IFVs:

- Glycol-water
- Hot water
- Hydrocarbon (propane, butane or mixed refrigerant)

The glycol-water option uses a glycol, such as ethylene glycol, propylene glycol or another low freezing point fluid to avoid freezing. Typically the glycol-water mixture delivers heat in a shell-and-tube heat exchanger. On the other side of the loop the mixture can receive heat from different heat sources, typically an air heater, reverse cooling tower, seawater, waste heat or a fired heater from a nearby industrial plant. The main advantage of the glycol-water scheme is that the intermediate fluid temperature can be controlled to be above freezing temperature of water to avoid icing.

The hot water option is usually used in a hybrid system in combination with a power or industrial plant, or another heat source at higher than ambient temperatures. For example, the hot exhaust gases from a gas turbine can heat water in a closed loop that vaporizes LNG on the cold side of the IF loop. The cold water flowing back from the LNG heat exchanger can be used to lower the turbine inlet temperature to increase efficiency. As the temperature of the heat source is high no glycol additives are needed.

Hydrocarbons can also be used to avoid the freezing problems often encountered with water. This arrangement allows the use of seawater as low as 1℃, compared to 5℃ with the ORV. Furthermore IFVs are often more compact than ORVs, because there is no direct contact between cryogenic LNG and seawater. Therefore IFVs are often preferable when considering floating LNG terminals. The arrangement will often, but not necessarily, make use of the latent heat of condensation of the intermediate fluid to vaporize the LNG. Seawater is usually used to evaporate and/or heat the intermediate fluid on the warm side of the IF loop, as well as heat the NG after it is evaporated in the primary heat exchanger. Thus direct contact between seawater and cryogenic LNG is avoided. This arrangement is shown in figure 7.

As with ORV's, this type of vaporizer requires substantial amounts of water and the water temperature drop is limited by environmental concerns. Kobe Steel Ltd. (company presentation, 2005) suggest a maximum temperature difference of 5.5℃.

Though all vaporizer types have their advantages, Xu et. al (2015) note that the IFV display better adaptability, and no icing problems, when compared to the ORV, better energy efficiency than the SCV (no natural gas consumed) and better robustness than AAV. The IFV is generally less sensitive to the ambient conditions, and is compact and therefore suitable for storage on vessels.

Xu et. al. (2015) compares several refrigerants as IFs for IFVs. They use a configuration where the refrigerants evaporate and condense, and found that the heat transfer area of the evaporator increases, while the area of the condenser decreases, with increased saturation temperature. The configuration used by Xu et. al. is shown below. For propane the total heat transfer area of the heat exchanger was about 3000 m^2. The calculations are supported by Pu et. al (2014) who further note that the largest thermal resistance was located in the thermolator (see fig. 7). The NG outlet temperature was increased with LNG inlet pressure, but is still limited by the thermolator and LNG mass flow.

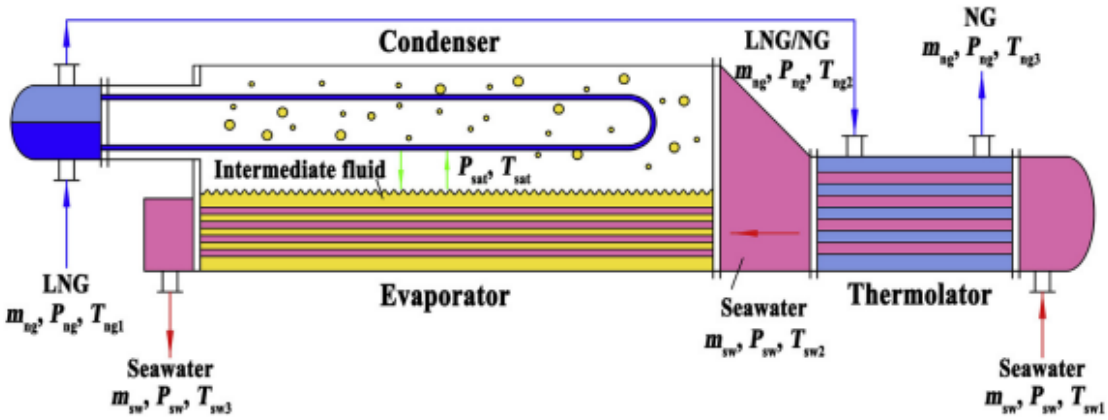

Figure 7: Shell and tube heat exchanger configuration for IFV

IFVs exist, and are in operation both on ships and land. Both glycol and propane are used in slightly different configurations, such as in a system delivered by Hamworthy Gas Systems AS (2010), which today is part of the Wärtsilä group. Hamworthy's system for glycol uses steam as a heat source to raise the glycol temperature to 90°C, which reduces the heat transfer area and leaves a compact system suitable for ship installation. The use of steam for the system, which was installed in USA, is mainly due to US restrictions on use of seawater. Hamworthy also produces a system with seawater as heat source and propane as IF. The propane is allowed to condense against LNG is evaporated in two parallel shell and tube heat exchangers against seawater.

A IFV regasification system is proposed by Liu et. al. (2013) using spiral-wound heat exchanger, and titanium in place of steel to increase conductive heat transfer. For the suggested system the heat transfer area was calculated to 1492m^2, significantly lower than for shell-and-tube heat exchangers.

2.2 LNG vaporizers in China

As described in figure 3 (list of China's major LNG terminals), several LNG terminals are already in place. The first one was operational in 2006, though there is still need for more, and more plants are in planning and construction (Lin et. al., 2010). Most of today's operational terminals utilize ORV with SCV for peak or cold periods. Two plants, in Shanghai and Zhejiang, use a combination of IFVs and SCVs, while the FSRU in Tianjin uses water steam from a nearby source (Correspondence w/ Prof. Lin W., 2014).

The LNG terminal in Putian is integrated with an air separation unit and is, to the authors knowledge, the only Chinese on-stream regasification facility that utilizes cold energy.

2.3 Heat exchanger correlations

Heat exchangers are widely used in industrial processes for various operations, such as heating, cooling, boiling or condensation. The heat exchanger studied in this project is a simple tube in tube heat exchanger part of a LNG regasification system with propane as intermediate fluid. The type is single by-pass and counter-current with no baffles or fins.

Heat exchanger efficiency is measured by the overall heat transfer coefficient, or by the amount of heat transferred per unit surface area. Pressure drop and surface area is used to calculate the capital and operating expenditures. This chapter will describe the relevant heat transfer correlations (Incropera et. al., 2006).

Heat transfer

Heat transfer occurs from the hot to the cold fluid. The overall heat balance of the heat exchanger can be written as

$$Q_h = m_h c_{p,h}(T_{h,i} - T_{h,o}) \tag{2.1}$$

$$Q_c = m_c c_{p,c}(T_{c,o} - T_{c,i}) \tag{2.2}$$

The subscripts *h* and *c* denotes the hot and cold fluid, respectively, and the subscript *i* and *o* denotes inlet and outlet, respectively. In truth, the heat released by the hot fluid will not equal the heat received by the cold fluid, as some heat is exchanged with the environment and some is lost to resistance due to wall fouling. However, these effects are usually small and deemed negligible, and heat exchangers are usually isolated well.

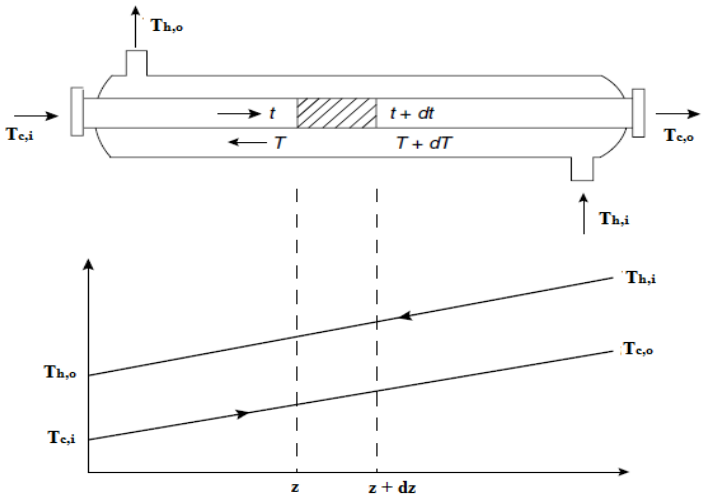

Figure 8: Tube-in-tube heat exchanger

With the assumptions of no fouling and fully isolated heat exchanger equations 2.1 and 2.2 are related by

$$Q = Q_c = Q_h \tag{2.3}$$

It is further assumed that the overall heat transfer coefficient and specific heat capacities are constant. The values may in truth change with temperature, but the change is negligible (Incropera et. al., 2006). With these assumptions the heat transfer can be expressed in terms of the overall heat transfer coefficient.

$$Q = UA\Delta T_{LM}\,, \tag{2.4}$$

ΔT_{LM} (also denoted LMTD) is the logarithmic mean temperature difference and is defined in equation 2.5 for counter-current heat exchangers, and illustrated by figure 9.

$$\Delta T_{LM} = \frac{(T_1 - t_2) - (T_2 - t_1)}{\ln\left(\frac{T_1 - t_2}{T_2 - t_1}\right)} \tag{2.5}$$

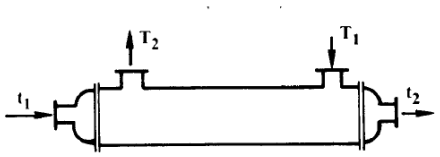

Figure 9: Counter-current LMTD configuration

Overall heat transfer coefficient

The overall heat transfer coefficient describes the ability to transfer heat across the relevant resistances. It may depend on the fluid properties, temperatures, flow rates and the geometry of the

heat exchanger. Geometry may include number of passes and baffles and their arrangements. The equation for the overall heat transfer coefficient is given below.

$$U = \frac{1}{\frac{1}{h_o} + R_{fo} + \frac{\Delta x_w}{k} + R_{fi} + \frac{1}{h_i}} \tag{2.6}$$

Δx_w and k are the wall thickness and thermal conductivity, respectively. Should other thermal resistances be present they may be added to the formula, for example fin resistance, contact resistance (if different materials are used) and so on. No further resistances are relevant for this thesis.

The film heat transfer coefficients are connected to the Nusselt number by equation 2.7:

$$h = \frac{Nu_L k}{L}, \tag{2.7}$$

where Nu_L is the Nusselt number and L is the characteristic length. The Nusselt number is a dimensionless number that describes the ratio between convective and conductive heat transfer. It is typically low (close to 1) for laminar flows, while turbulent flows are typically in the 100-1000 range. For turbulent flow in a pipe the Nusselt number is related to the Reynolds (Re) and Prandtl (Pr) numbers by the Dittus-Boelter equation:

$$Nu_L = 0.023 \mathrm{Re}^{0.8} \mathrm{Pr}^n \tag{2.8}$$

The constant n is 0.4 for heating and 0.33 for cooling, and the correlation is valid for Prandtl numbers from 0.6 to 160. The Reynolds and Prandtl numbers may be found by their standard equations:

$$\mathrm{Re} = \frac{\rho U L}{\mu} \tag{2.9}$$

$$\mathrm{Pr} = \frac{c_p \mu}{k} \tag{2.10}$$

3.0 Cold energy recovery feasibility study

Cold energy is associated with the regasification of LNG to such an extent that utilization of this energy in various ways may be cost-effective. Several methods to extract and utilize the cold energy exist, though only the LNG terminal in Putian employs any form of cold energy utilizations in China. The Putian terminal is integrated with an air separation unit (ASU) and is producing 600 tpd of liquid oxygen, nitrogen and argon (GB Foster Wheeler, 2012). This chapter describes some possible cold energy utilization applications and a feasibility study for a propane-Rankine power generation cycle integrated with a LNG IF regasification system. The feasibility study is relevant for the next stage of research on the IF regasification system at SJTU, which will involve phase-changing propane as intermediate fluid.

As mentioned several technologies already exist for cold energy utilization. The most common method for utilization is by an ASU; the ASU is integrated in the LNG terminal in such a way that the ASU utilizes the vaporizing LNG as a heat sink. In the same way cold energy can be utilized for district cooling or freezing, chilled water for industry, dry ice manufacturing or regasification of boil-off gas. Usually the heat is transferred by a suitable heat transfer fluid, for example a water-glycol mixture. Another efficient method of cold energy utilization is inlet air cooling for gas turbines. By cooling the air to sub-ambient temperatures gas turbines can increase their efficiencies. GB Foster Wheeler (2012) claims that for every lowered degree Celsius of inlet air temperature, the power output from a gas turbine is increased by 0.5%, and further that an inlet air-cooling integrated system has a pay-back of three years. Niche applications of cold energy utilization include cryogenic crushing and seawater desalination.

Finally, the subject of this feasibility study is the Rankine power cycle for cold energy utilization. Power generation can potentially not only cover the energy cost of a LNG terminal but produce a surplus of power. It is proposed that *"when LNG is pumped to 100 barg or higher, heated and expanded to 30 barg, a significant amount of power can be generated"* (Patel et. al.,2013). In large plants the power generation may eliminate power import, which largely reduces cost. GB Foster Wheeler (2012) claims that a 5 MTPA plant will have about 110 MW of cold energy available, and about 35 MW extractable by the Rankine cycle method. In the cycle the intermediate fluid of the IMF vaporizer boils against seawater at a high pressure, expands to a lower pressure and condenses against LNG. Propane is a suitable fluid for this cycle. The general Rankine cycle method is shown in figure 9. Note that the NG is expanded after the seawater trim heater and thus contributes to the power output.

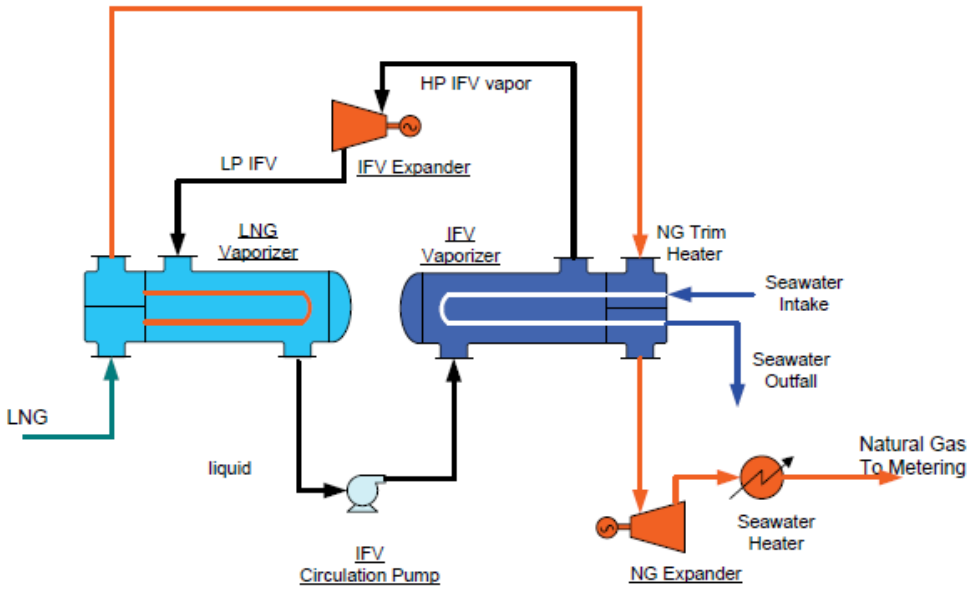

Figure 10: Intermediate fluid vaporizer with Rankine cycle

A Hysys simulation has been conducted for a LNG IFV regasification system with propane. The system is depicted in figure 10 below. It is a quite simple and straightforward attempt at cold energy utilization. The LNG is pumped to 100 bar as proposed by Patel et. al. (2013), heated by propane, vaporized by seawater and expanded to 30 bar. Note that the LNG is vaporized in the water heat exchanger (F-102), in accordance with the setup by Foster Wheeler and unlike the process in figure 9. This is due to the high LNG pressure.

The propane runs in a loop from point 1 to 7. It is condensed by LNG and exits the heat exchanger as saturated liquid at 0.1 bar and -84°C, before being pumped to 3.6 bar. It is then evaporated by water and exits the heat exchanger as gas at 3.5 bar and -9°C. A two-stage turbine with intermediate water heating reduces the pressure to 0.1 bar at stage 7/1. At this point the temperature is -60°C. The adiabatic efficiencies of all turbines are set to 75%.

Note that all adjust and optimizing tools used in Hysys have been removed from the system in figure 10, to better allow the reader to understand the setup. Furthermore water pumps have not been included in this simulation. Some limitations have been set: the minimum temperature approach is 10°C in all heat exchangers, which limits the mass flow of propane by temperature approach in the LNG heat exchanger (LNG-100). The water inlet temperature is 20°C, and the outlet temperature 5°C. The pressure drop has, for simplicity, been set to 0.1 bar in all heat exchangers.

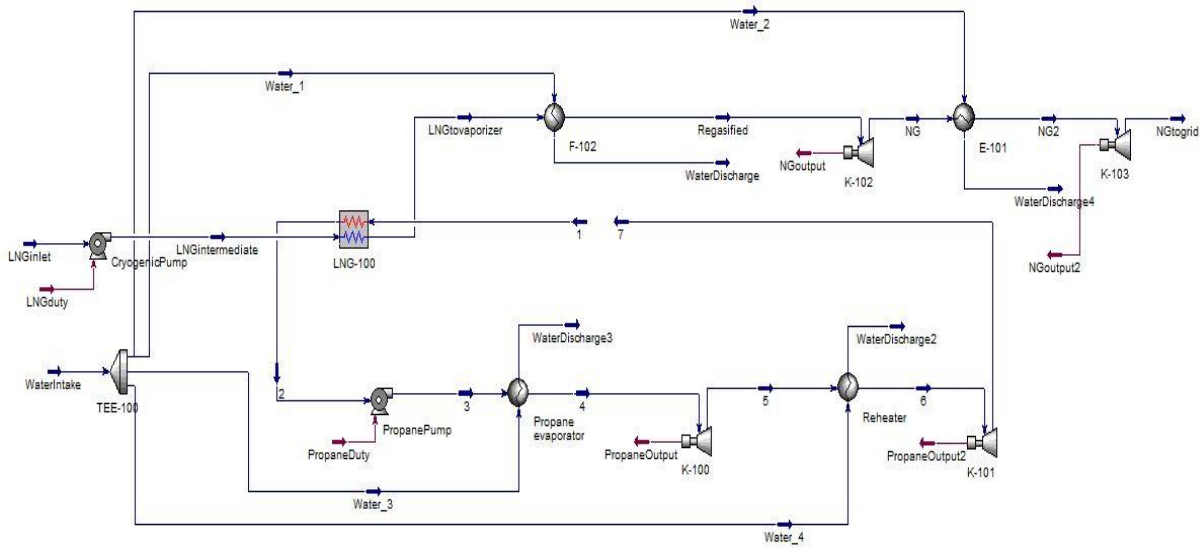

Figure 11: HYSYS simulation layout

The process produces 22..139 MW and consumes 4.548 MW, mainly for pumping the cryogenic LNG from 1 to 100 bar. Water consumption is high; the total flowrate of water is 63.7 MTPA for 5 MTPA of LNG. As previously stated large consumptions of seawater can potentially affect the surrounding environment by lowering the temperature, which should be avoided. The net power production is 17.5 MW, quite far off from the 32 MW that Foster Wheeler claims is possible. However it should be noted that this study does not employ a complicated model. The purpose is only to investigate the possibility of power production and the simulation model can be improved to a great extent. 17.5 MW for a 5 MTPA LNG terminal justifies the installation of a cold energy utilization system, in terms of both process engineering and economics. The calculations agree with a study by Szargut & Szczygiel (2009), who claim that the investment cost of a simple plant is 593.9 $/kW and the payback time of the plant would be 6.4 years.

The system can be improved in several ways. For example, the turbine configuration can be optimized. The pressure drop across each expander stage can be adjusted to possibly increase the power output and more stages than two can be included. Intermediate stages are calculated on the basis of the inlet conditions and can possibly be changed in favor of more power production. Further optimization work may increase the power output as well as reduce the water consumption. Every heat exchanger except the LNG heat exchanger employ the simple weighted heat exchanger model, which is quite simple. A more detailed study should use more accurate models to calculate both the heat transfer and the pressure drop.

For large plant (more than 5 MTPA) applications it may also be interesting to investigate expansions of the simple Rankine cycle to make further use of the cold energy. One such system is the binary working fluid and absorption process proposed by Yanni Liu & Kaihua Guo (2010), which use propane and tetrafluoromethane (CF_4) as working fluids. The Rankine cycle in different variations in cold energy utilization can be a thesis topic alone, and is somewhat of a digression to this thesis. Therefore any further work on this branch of LNG terminals will be left to other students at SJTU.

4.0 Mathematics of CFD simulations

FLUENT allows the choice between several mathematical models to simulate turbulent flow. These models as well as the underlying governing equations will be briefly explained in this chapter, as well as the relevant wall treatment methods.

4.1 Governing equations

4.1.1 Continuity equation

The continuity equation is a mathematical statement that describes the transport of a conserved quantity. In the case of fluid dynamics at steady state this quantity is fluid density, denoted ρ. The equation states that the transported quantity in question is locally conserved. In the case of fluid density it can be said that the rate at which mass enters the system is equal to the rate at which mass exits the system. This is expressed mathematically as:

$$\frac{\partial \rho}{\partial t} + \nabla \cdot (\rho U) = 0 , \tag{3.1}$$

where t is time, U is the flow velocity vector field and ∇ is the del operator. With the divergence term written out the full equations reads:

$$\frac{\partial \rho}{\partial t} + \frac{\partial \rho U_1}{\partial x_1} + \frac{\partial \rho U_2}{\partial x_2} + \frac{\partial \rho U_3}{\partial x_3} = 0 \tag{3.2}$$

The assumption that the flow is incompressible will remove the first term of the equation. It is valid for most engineering applications and simplifies the model to a great extent. The assumption is valid even for gases because a local change in pressure will spread with the speed of sound. When the modelled flow is much slower than the speed of sound, as is certainly the case in this project, the new pressure will be reached in one time-step. Thus the variation of gas density due to pressure waves can be ignored (Andersson et. al., 2011). The density change due to other factors, namely pressure drops and temperature variations, is compensated for by the state equation relating density to temperature and pressure.

4.1.2 Momentum equation (Navier-Stokes)

The momentum equations, of which one form is referred to as the Navier-Stokes equations, arise from Newton's second law; the change in momentum in any direction is equal to the sum of forces acting in that direction. The two groups of forces acting on a finite volume are body forces and surface forces. Body forces include gravity, centrifugal and electro-magnetic forces, while surface forces include pressure and viscous forces. The general tensor form of the equation is given as:

$$\frac{\partial U_1}{\partial t} + U_j \frac{\partial U_i}{\partial x_j} = -\frac{1}{\rho}\frac{\partial P}{\partial x_i} + \frac{1}{\rho}\frac{\partial \tau_{ij}}{\partial x_j} + g_i, \tag{3.3}$$

For which i and j denotes the Cartesian dimensions. The left side describes acceleration, both time-dependent and convective, whereas the right side is the summation of body and surface forces.

The continuity equation is hard to solve numerically and is therefore often combined with the momentum equation to form the Poisson equation, which has better numerical properties. This equation treats pressure as a dependent variable and the momentum equations are formulated to solve for velocity (Andersson et. al., 2011). For constant viscosity and density, it is given as:

$$\frac{\partial}{\partial x_i}\left(\frac{\partial P}{\partial x_i}\right) = -\frac{\partial}{\partial x_i}\left[\frac{\partial(\pi U_i U_j)}{\partial x_j}\right] \tag{3.4}$$

4.1.3 Energy equation

Energy exists in various forms in fluid flow. The components of the total energy of a system is kinetic, potential, thermal and chemical energy, denoted respectively below in terms of enthalpy *h*.

$$\begin{aligned} h_m &= \frac{1}{2}\rho U_i^2 \\ h_T &= \sum_n m_n \int_{T_{ref}}^{T} c_{p,n} dT \\ h_C &= \sum_n m_n h_n \\ h_\phi &= \rho g_i x_i \end{aligned}, \tag{3.5}$$

where m_n is the mass fraction, c_p is the heat capacity and h_n is the enthalpy of formation for species n. The total heat balance for the system is given below.

$$\frac{\partial h}{\partial t} = -\frac{\partial}{\partial x_j}\left[hU_j - k_{eff}\frac{\partial T}{\partial x_i} + \sum_n m_n h_n j_n - \tau_{kj} U_k\right] + S_h \tag{3.6}$$

J_n is the diffusional flux for species *n* and *S* is a source term. For incompressible flows the couplings between the different parts of the energy balance are weak, and the balance equations for kinetic and thermal energy be written separately (Andersson et. al., 2011). There is no transport of chemical energy in this project and potential energy is included in the kinetic balance. The equation for kinetic energy is given below.

$$\frac{\partial(h_m)}{\partial t} = -U_j \frac{\partial(h_m)}{\partial x_j} + P\frac{\partial U_i}{\partial x_i} - \frac{\partial(PU_i)}{\partial x_i} - \frac{\partial}{\partial x_j}(\tau_{ij}U_i) - \tau_{ij}\frac{\partial U_i}{\partial x_j} + \rho g U_i \tag{3.7}$$

The first two terms on the right are accumulation and convection terms and the third term is reversible conversion to heat from thermodynamic cooling from gas expansion or heating from gas compression. The fourth term accounts for work done by viscous forces, the fifth for irreversible conversion of kinetic energy to heat and the sixth term is the work done by gravity force, i.e. the change in potential gravity. Similarly the energy equation for thermal energy can be devised by adding the source terms from the kinetic energy equation.

$$\frac{\partial(\rho \mathrm{C}_p \mathrm{T})}{\partial t} = -U_j \frac{\partial(\rho \mathrm{C}_p \mathrm{T})}{\partial x_j} + k_{eff}\frac{\partial^2 T}{\partial x_j x_j} - P\frac{\partial U_j}{\partial x_j} + \tau_{kj}\frac{\partial U_k}{\partial x_j} \tag{3.8}$$

The right-hand terms in order from left to right are for accumulation, convection, conduction and expansion.

4.2 Turbulence modelling

Turbulent flow is a phenomena characterized by chaotic and random property changes. At the onset of turbulence the viscous dampening of the velocity fluctuations will be slower than the convective transport, which allows the fluid elements to rotate before it comes in contact with a wall that stops the rotations. The turbulent flow has a wide range of length, velocity and time scales, for which the solution demands a high cost of simulation (Andersson et. al., 2011). To reduce the cost several turbulence models of varying resolution have been developed, all making simplifications to the previously discussed governing equations. Intuitively direct numerical solution (DNS) might be the best approach. However, it requires a huge amount of computational power. Large eddy simulation (LES) is a model that provides detailed information about structures in turbulent flow, but still requires a great amount of data to be stored and post-processed. With the present-day available computational power, time-averaged Reynolds equations (RANS) are usually deemed sufficiently accurate. The difference is illustrated below.

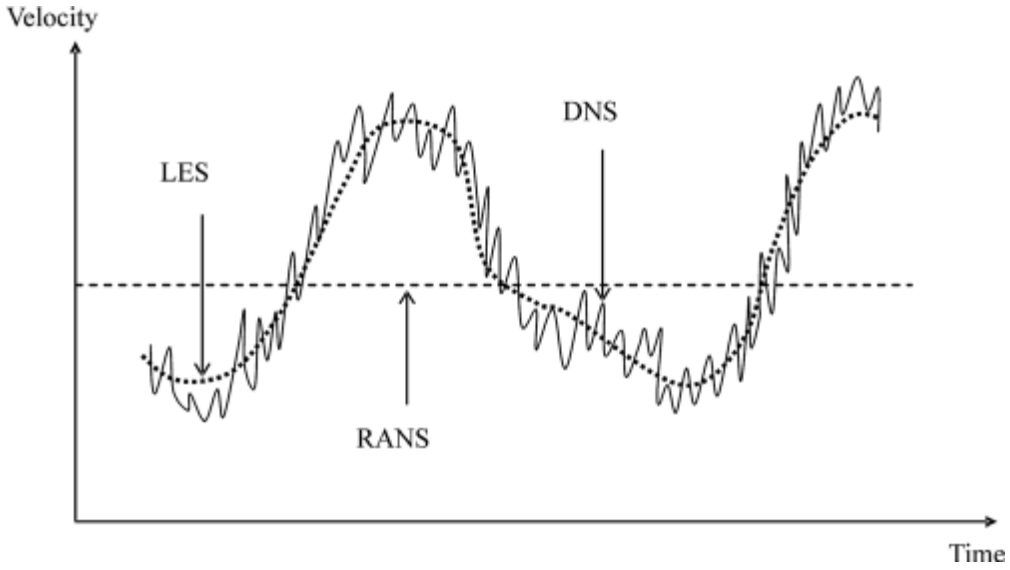

Figure 12: Turbulence models

The RANS model, as proposed by Reynolds in 1895, splits the instantaneous variables into a mean and a fluctuation part.

$$U_i = \langle U_i \rangle + u_i$$
$$P = \langle P_i \rangle + p_i \tag{3.9}$$

This method, referred to as Reynolds decomposition, is the basis for all of the turbulence models discussed in this project. For compressible flows the density has to be decomposed as well. Inserting these equations into the Navier-Stokes and continuity equations and rearranging gives the Reynolds averaged Navier-Stokes equation,

$$\frac{\partial \langle U_i \rangle}{\partial t} + \langle U_i \rangle \frac{\partial \langle U_i \rangle}{\partial x_j} = -\frac{1}{\rho}\frac{\partial}{\partial x_j}\left[\langle P \rangle \delta_{ij} + \mu\left(\frac{\partial \langle U_i \rangle}{\partial x_j} + \frac{\partial \langle U_j \rangle}{\partial x_i} \right) - \rho \langle u_i u_j \rangle \right] \tag{3.10}$$

Note the term $-\rho\langle u_i u_j \rangle$, which is the Reynolds stresses, introducing a coupling between the mean and fluctuating parts of the decomposition. This term is unknown and must be modelled to solve the equation, which is done by expressing the Reynolds stress in terms of mean velocity. The Boussinesq approximation is the resulting equation (Andersson et. al., 2011), which reads

$$\frac{\tau_{ij}}{\rho} = -\langle u_i u_j \rangle = \upsilon_T \left(\frac{\partial \langle U_i \rangle}{\partial x_j} + \frac{\partial \langle U_j \rangle}{\partial x_i} \right) - \frac{2}{3} k \delta_{ij} . \tag{3.11}$$

τ_{ij} is the Reynolds stresses, υ_T is the eddy viscosity and k is the turbulent kinetic energy. The Boussinesq approximation assumes that all eddies behave like molecules, that turbulence is isentropic and that stress and strain is in local equilibrium. Despite that such assumptions may be incorrect, most turbulence models are based on these approximations. To use the RANS model, the Boussinesq approximation is often given with additional transport equations for turbulence kinetic energy k, and either turbulence dissipation rate ε or the specific dissipation rate ω. This provides the two-equation models that are to be discussed in this chapter, namely the $k-\varepsilon$ models and the $k-\omega$ models.

4.2.1 Two-equation models

Standard $k-\varepsilon$ model

Among the two-equation models, the $k-\varepsilon$ model is the most commonly employed. It provides a good compromise between accuracy and economy. There are three different models: the standard, the realizable and the RNG $k-\varepsilon$ model. All three equations try to describe the transport of k and ε. For the standard $k-\varepsilon$ model the transport equations are given below.

For k: $$\frac{\partial k}{\partial t} + \langle U_j \rangle \frac{\partial k}{\partial x_j} = \upsilon_T \left[\left(\frac{\partial \langle U_i \rangle}{\partial x_j} + \frac{\partial \langle U_j \rangle}{\partial x_i} \right) \frac{\partial \langle U_i \rangle}{\partial x_j} \right] - \varepsilon + \frac{\partial}{\partial x_j}\left[\left(\upsilon + \frac{\upsilon_T}{\sigma_k} \right) \frac{\partial k}{\partial x_j} \right] \tag{3.11}$$

For ε: $$\frac{\partial \varepsilon}{\partial t} + \langle U_j \rangle \frac{\partial \varepsilon}{\partial x_j} = C_{\varepsilon 1} \upsilon_T \frac{\varepsilon}{k}\left[\left(\frac{\partial \langle U_i \rangle}{\partial x_j} + \frac{\partial \langle U_j \rangle}{\partial x_i} \right) \frac{\partial \langle U_i \rangle}{\partial x_j} \right] + C_{\varepsilon 2} \frac{\varepsilon^2}{k} + \frac{\partial}{\partial x_j}\left[\left(\upsilon + \frac{\upsilon_T}{\sigma_\varepsilon} \right) \frac{\partial \varepsilon}{\partial x_j} \right] \tag{3.12}$$

The left hand terms of the equations are accumulation and convection by mean velocity of the transported variable. The right hand terms are from left to right production, dissipation and diffusion of the transported variable. The robustness and simplicity of the model makes it the most widely used of the two-equation models. However, the accuracy is not very good for certain conditions; it is aimed at high Reynolds numbers, where the flow is nearly isotropic and in accordance with the assumptions of the Boussinesq approximation (Andersson et. al., 2011) (Ansys FLUENT user guide, 2015). Several improvements of the model have been proposed, of which the RNG and realizable $k-\varepsilon$ models are the best known.

RNG $k-\varepsilon$ model

In the RNG $k-\varepsilon$ model a source term is added to the dissipation equation. The term is denoted S_ε and the equation becomes

$$\frac{\partial \varepsilon}{\partial t}+\langle U_j\rangle\frac{\partial \varepsilon}{\partial x_j}=C_{\varepsilon 1}\upsilon_T\frac{\varepsilon}{k}\left[\left(\frac{\partial\langle U_i\rangle}{\partial x_j}+\frac{\partial\langle U_j\rangle}{\partial x_i}\right)\frac{\partial\langle U_i\rangle}{\partial x_j}\right]+C_{\varepsilon 2}\frac{\varepsilon^2}{k}+\frac{\partial}{\partial x_j}\left[\left(\upsilon+\frac{\upsilon_T}{\sigma_\varepsilon}\right)\frac{\partial \varepsilon}{\partial x_j}\right]-S_\varepsilon,$$

$$S_\varepsilon=2\nu S_{ij}\left\langle\frac{\partial u_1}{\partial x_i}\frac{\partial u_1}{\partial x_j}\right\rangle \qquad \text{(3.13) and (3.14)}$$

The addition of the extra source term of the RNG $k-\varepsilon$ model results in a smaller destruction of the dissipation rate ε in regions with large strain rate. The RNG model models swirling flows well, and is more responsive to the effects of rapid strain and streamline curvature.

Realizable $k-\varepsilon$ model

The realizable model differs from the standard by imposing a realizable constraint on the Reynolds stress tensor. The stress term in the normal model can become negative and thus cause errors. In the realizable model the term is modelled as

$$\langle u_i u_j\rangle=\sum_i\langle u_i^2\rangle=\frac{2}{3}k-2\upsilon_T\frac{\partial\langle U_i\rangle}{\partial x_j} \qquad (3.15)$$

The stress tensor must now be larger than zero by definition as it is the sum of squares. Thus the model provides better performance when modelling rotation and separation. The realizable $k-\varepsilon$ model is more reliable in its treatment of boundary layer flows, separated flows and rotating shear flows, and generally regarded as a solid improvement to the standard model.

Standard $k-\omega$ model

In this model the specific turbulence dissipation ω is used as the length-determining variable. The transport equations for k and ω are given below.

$$\frac{\partial k}{\partial t}+\langle U_j\rangle\frac{\partial k}{\partial x_j}=\upsilon_T\left[\left(\frac{\partial\langle U_i\rangle}{\partial x_j}+\frac{\partial\langle U_j\rangle}{\partial x_i}\right)\frac{\partial\langle U_i\rangle}{\partial x_j}\right]-\beta k\omega+\frac{\partial}{\partial x_j}\left[\left(\upsilon+\frac{\upsilon_T}{\sigma_k}\right)\frac{\partial k}{\partial x_j}\right] \quad (3.16)$$

$$\frac{\partial \omega}{\partial t}+\langle U_j\rangle\frac{\partial \omega}{\partial x_j}=\alpha\frac{\omega}{k}\upsilon_T\left[\left(\frac{\partial\langle U_i\rangle}{\partial x_j}+\frac{\partial\langle U_j\rangle}{\partial x_i}\right)\frac{\partial\langle U_i\rangle}{\partial x_j}\right]-\beta^*\omega^2+\frac{\partial}{\partial x_j}\left[\left(\upsilon+\frac{\upsilon_T}{\sigma_\omega}\right)\frac{\partial \omega}{\partial x_j}\right] \quad (3.17)$$

This model has a major advantage when k and ε approach zero, in areas with low turbulence. It has also accurately predicted the law on the wall in the viscous sub-layer, eliminating the need for wall functions. The $k-\varepsilon$ models usually require a low-Re number modification in this area. However, the $k-\omega$ model requires a fine mesh close to the wall with a low y+ of about 1.

SST $k-\omega$ model

The shear stress transition (SST) $k-\omega$ model blends the accurate and robust standard $k-\omega$ in the near wall region with the freestream independence of the $k-\varepsilon$ further form the wall. The $k-\varepsilon$ function is converted to a $k-\omega$ formulation. Both models are multiplied by a blending function, in which the blending function is equal to 1 near the wall which activates the $k-\omega$ model, and zero some prescribed distance from the wall which activates the $k-\varepsilon$ model. This feature makes the SST model more accurate and reliable for a wider class of flows, such as adverse pressure gradients and airfoils (Ansys FLUENT user guide, 2015).

4.3 Near-wall modelling

In many engineering applications the flow may be constrained by a wall. In the case of near-wall flow viscous effects on transport processes may be large, due to the wall no-slip condition, and a rapid variation of the flow variables may occur. To accurately capture the high gradients of flow variables a very fine mesh grid is needed, which raise problems. Mainly two solutions are developed to solve the near-wall area. The viscous region may not be resolved by the turbulence models, but are instead solved by wall functions that obtain the mean velocity components at the first grid point far from the wall. The other approach is to modify the turbulence models to allow the near-wall models to be resolved, usually with a relatively fine mesh. The difference between the two approaches is illustrated below.

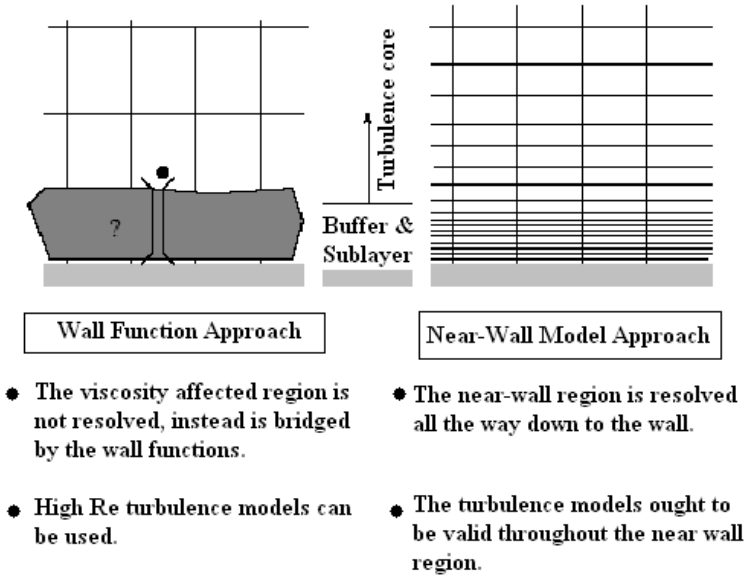

Figure 13: Near-wall modelling

4.3.1 Wall functions

Wall functions estimate the transported variables, such as velocity, temperature and pressure, from the first cell close to the wall to the turbulent boundary layer. They also formulate the turbulence variables, k and ε or ω based on the turbulence model in use. The functions are empirical formulas based on the law on the wall. The main types of wall functions in use are:

- Standard wall functions
- Scalable wall functions
- Non-equilibrium functions

Standard wall functions

The average velocity in the interior viscous boundary layer is given in the general form as

$$\langle U_i \rangle = f(y^+) \tag{3.18}$$

Certain steps are taken to obtain the logarithmic law of the wall; the total stress is assumed to be constant, the turbulent stresses to be negligible and the no-slip boundary condition is applied. This reduces the total stress tensor to $\tau_{xy} = -\rho \langle u_x u_y \rangle$. The tensor is introduced with Prandtl's mixing model and the equation is squared and integrated to obtain the logarithmic velocity profile in the dimensionless form (Andersson et. al., 2011) given as

$$\langle U_x \rangle^+ = \frac{1}{\kappa} \ln(y^+) + B \ , \tag{3.19}$$

where κ and B are constants. The equation is often referred to as the log law. In the viscous sub-layer the mean velocity varies linearly with y^+, while in the transition buffer layer it approaches the log law, as shown below.

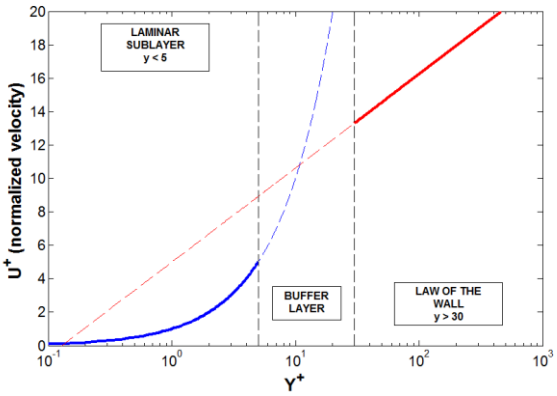

Figure 14: Law of the wall

When applying the wall functions the grid point that is closest to the wall should be in the logarithmic region. That is, if the grid is too close to the wall and in the laminar sublayer, the transition to the logarithmic region will happen in the turbulent region. Ideally the first grid point should be close to the buffer layer, which is $30 < y^+ < 100$.

Scalable wall functions

The scalable wall functions are an alternative to the standard that forces the use of the log law by displacing the y^+ in regions where it is smaller than 11.225. In FLUENT the transition between the linear and log regimes occurs at this value. In regions with a y^+ higher than 11.225 the scalable functions will give the same results as the standard functions.

Non-equilibrium wall functions

The standard wall functions assume an equilibrium between turbulence production and dissipation and constant shear. This assumption is not applicable if the flow experiences adverse pressure gradients at the boundary layer, because the fluid closest to the wall is retarded resulting in wall shear stress reduction. Consequently the mean velocity profile will be altered and the log law cannot be used. The accuracy of the standard wall functions for several types of flow, such as impinging flow or separation and re-attachment, will be low. The modified, non-equilibrium functions are to a greater extent capable of capturing such effects by relaxing the equilibrium condition. The wall functions consist of a log-law for the mean velocity which is responsive to pressure-gradient effects.

4.3.2 Enhanced wall treatment

Enhanced wall treatment concerns the second type of near-wall modelling approach, and is not a wall function itself. The technique permits solving the equations of the turbulence model all the way to the wall, but require a fine mesh resolution near the wall and thus higher computational power to do so. The improved modelling is achieved using a two-layer zonal approach or low-Reynolds number turbulence models. Both require roughly the same boundary layer mesh resolution.

Two-layer zonal modelling

As the name implies this method divides the near-wall region into two zones. They are identified by the wall-distance based Reynolds number, where y is the distance to the wall.

$$\mathrm{Re}_y = y\frac{\sqrt{k}}{\nu} \tag{3.20}$$

The viscosity-dominated region is taken to be at Reynolds numbers smaller than 200, while the fully turbulent region at higher numbers (Andersson et. al., 2011). In the low-Re region a one-equation turbulence model is applied to calculate the turbulent kinetic energy and an algebraic correlation is used to calculate the energy dissipation rate. In the fully turbulent zone the turbulence model is applied as normal. The viscous zone energy dissipation is calculated from

$$\varepsilon = \frac{k^{3/2}}{l_\varepsilon}, \tag{3.21}$$

where l_ε is the appropriate length scale. A blending function is usually employed to calculate a smooth transition between the two zones.

Low-Reynolds number turbulence model

This approach differentiates between high and low Reynolds number areas. The $k-\varepsilon$ models are an example of a high Reynolds number model, which as previously stated are not valid for near-wall fluid flows where viscous forces are dominant. Low-Reynolds number models can, however, be resolved all the way to the wall. These models are modified by adding dampening functions for the source terms in the ε-equation and for the expressions of turbulent viscosity. Note that for high global Reynolds numbers a transition model is needed. The transport equations for k and ε read

$$\frac{\partial k}{\partial t}+\langle U_j\rangle\frac{\partial k}{\partial x_j}=\frac{\partial}{\partial x_j}\left[\left(\upsilon+\frac{\upsilon_t}{\sigma_k}\right)\frac{\partial k}{\partial x_j}\right]+\upsilon_t\left[\left(\frac{\partial\langle U_i\rangle}{\partial x_j}+\frac{\partial\langle U_j\rangle}{\partial x_i}\right)\frac{\partial\langle U_i\rangle}{\partial x_j}\right]-\varepsilon \tag{3.22}$$

$$\frac{\partial \varepsilon'}{\partial t}+\langle U_j\rangle\frac{\partial \varepsilon'}{\partial x_j}=\frac{\partial}{\partial x_j}\left[\left(\upsilon+\frac{\upsilon_t}{\sigma_\varepsilon}\right)\frac{\partial \varepsilon'}{\partial x_j}\right]+C_{1\varepsilon}f_1\upsilon_t\frac{\varepsilon'}{k}\left[\left(\frac{\partial\langle U_i\rangle}{\partial x_j}+\frac{\partial\langle U_j\rangle}{\partial x_i}\right)\frac{\partial\langle U_i\rangle}{\partial x_j}\right]-C_{2\varepsilon}f_2\frac{\varepsilon'^2}{k}+E$$

(3.23)

The turbulent viscosity is calculated from

$$\upsilon_t=f_\mu C_\mu\frac{k^2}{\varepsilon'}, \tag{3.24}$$

and the energy dissipation is related to ε' by $\varepsilon=\varepsilon_0+\varepsilon'$. ε_0 is the value of the dissipation at the wall. The damping functions are denoted f_1, f_2 and f_μ (Andersson et. al., 2011).

5.0 Experimental setup

A test rig has been built at the Jiao Tong University. The rig is a small modification of a rig previously used by other students for similar experiments. The rig is built as a simple, small-scale regasification unit with two tube-in-tube heat exchangers. The rig flow chart is shown in figure 17 and a picture of the isolated and finished rig is shown below in figure 15. As indicated on the picture, the nitrogen heat exchanger is the top horizontal pipe, while the water heat exchanger is the lower horizontal. For the heat exchanger dimensions, please refer to chapter 5.1. A more detailed description of the experimental set-up and procedure can be found in appendix 1, while the laboratory log is found in appendix 2.

Figure 15: Laboratory rig.

Instrumentation	Position
Water heater	Large white box behind computer screen
Temperature sensors	At inlets and outlets and along length of heat exchangers. All marked “T1” in process flow diagram.
Pressure sensors	At IF inlets. Value recorded as seen in red on the signal processing devices placed on top of the water heater. Both marked “P1” in process flow diagram

Flow meters	Not seen in picture Placed on pipes upstream of inlets. See process flow diagram
C3 and N2 tanks	Outside laboratory. Not seen in picture. Nitrogen is vented to atmosphere

Figure 16: Instrumentation positions

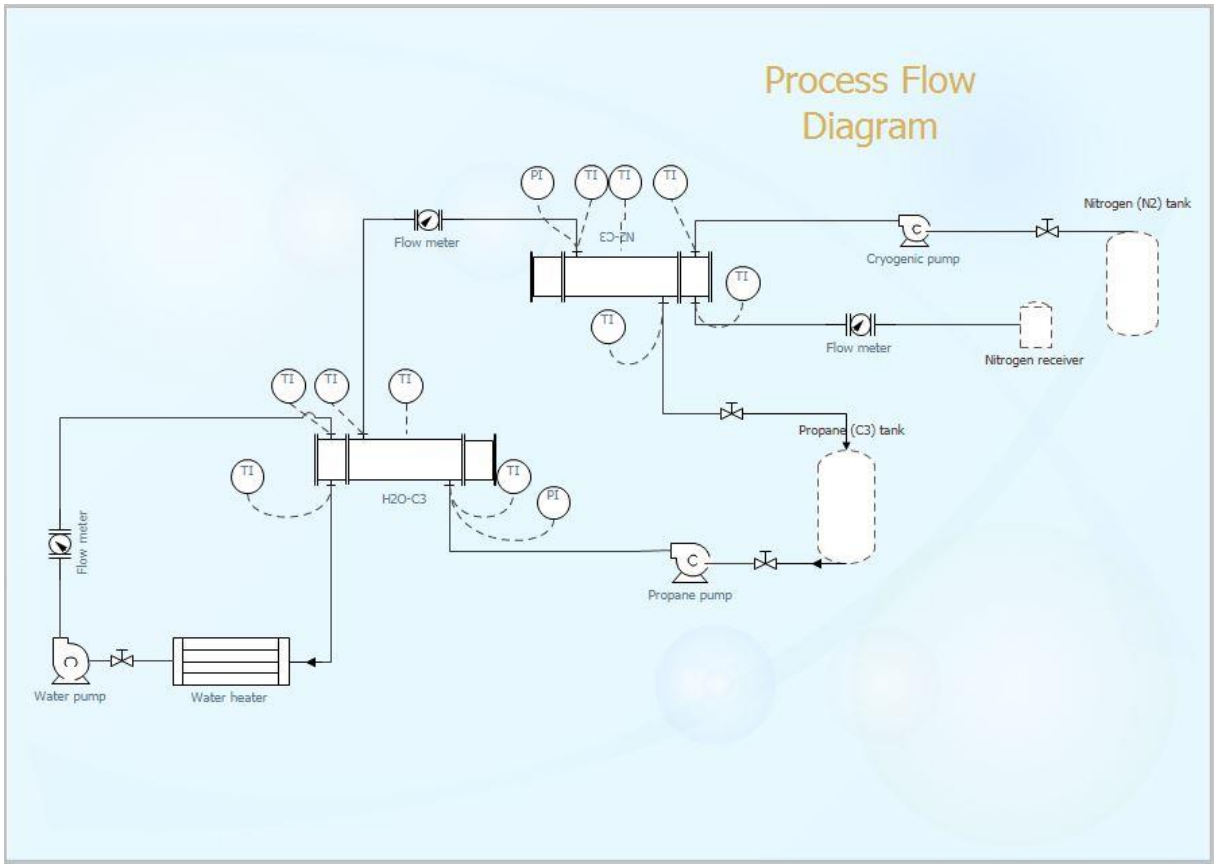

Figure 17: Experiment layout

Figure 18: Thermocouple sensor

5.1 Sensors

Sensors are installed to continuously monitor temperature, pressure and flowrate of the three fluids. The following chapters will proved an outline of the sensor set-up, installation, calibration and error analysis.

5.1.1 Temperature

Temperature is recorded by PT-100 thermocouple sensors. Figure 18 shows a picture of one of the sensors. The temperature junction is found at the tip of the housing, which is screwed into holes drilled on the heat exchangers. There is one sensor installed at each outlet and inlet, and 5 sensors along the length (x –axis) of each heat exchanger in the outer (IF) tube. This will provide the measurement of the IF temperature profile along the heat exchangers and the total heat transfer. There are 18 sensors in total.

As stated the thermocouples are screwed into pre-bored holes on the heat exchangers. The wires are then extended and connected to a Keithley 2701 multimeter, which process the electrical signals. The sensors are 4-wire type thermocouples. Because the multimeter has 22 channels only, with two connections each, two and two wires were soldered together for each sensor. The length of the extension wires range from 1 to 3 meters.

The default inaccuracy for each sensor is 0.1 K and the signal output for each sensor from the multimeter is given as resistance in ohm. With each sensor the manufacturer has provided a data sheet with resistances and corresponding temperatures, slightly different for each sensor. The relationship between resistance and temperature is assumed to be linear. The resistance to temperature data is entered into excel and by linear regression the relationship function is found for each sensor. This data can be found in the excel data sheet named “relationships”, appendix 3. The assumption of linearity will increase the error of the sensor by maximum 0.2 K.

Next, the extension wires are found to have approximately 0.4 ohm resistance per meter. Considering the length of the wires (up to 3 m) and that a change of 0.4 ohm amounts to roughly 1 degree (depending on the sensor), the added resistance is significant. The wire resistance is deducted from the recorded value in excel. Finally the sensors are calibrated against room temperature. Room temperature is measured by a mercury-in-glass thermometer (+-0.1 K). Modifications were done in excel to add or subtract resistance until all sensors displayed the same temperature +- 0.05 K. This process was repeated several times, until the sensors all gave a repeatable temperature reading equal to the recorded room temperature +- 0.6 K. This calibration process was only conducted at times with stable ambient temperature (afternoon, stable weather) and over 3 consecutive days. The

calibration was also controlled in between experiments and found to be within the limits. The final accuracy of the thermocouple sensors is +-0.6 K.

5.1.2 Pressure

Pressure is recorded for the intermediate fluid at the inlets of both heat exchangers. The main purpose of the pressure measurement is to control that propane is in liquid state, which require pressure in the range of 0.6-0.7 MPa, depending on temperature. The pressure sensor type is NS-P-I and it is a piezoelectric sensor. The range is 1 MPa and the error is 0.25%.

The pressure sensors are both pre-calibrated by the manufacturer and no further calibration is needed. The recorded pressure is in agreement with pressure gauges on the tank.

5.1.3 Flowrate

3 flowrate sensors are employed, one for each fluid loop. The flow is undisturbed for more than 10 pipe diameters upstream of each flowmeter. The IF and water flowrates are of the same type (LWGY-15BBRS1/E/NE/NT) and both have an error of 0.5%, while the nitrogen flowmeter is of the type HSM-015YES1AB1/EX and has an error of 1%. The flow meters are all of the turbine type.

5.2 Boundary conditions

Efforts are made to conduct all experiments at similar, if not equal, conditions. The boundary conditions for the experiments will herein be explained along with any complications, as well as some suggestions for improvements.

The nitrogen is fed at 1 barg from the tank as liquid. However, the heat in-leak along the pipe from the tank to the first heat exchanger is high and the nitrogen is gaseous at the inlet. The mass flow is kept high relative to the other fluids to maintain a low and stable temperature. The flow rate was controlled by the outlet valve at the tank, a standard bell valve. The flowrate was hard to control and it was near impossible to achieve the same flowrate after closing and re-opening the valve. Furthermore the nitrogen flow meter value proved to be fluctuating, even though the valve was strictly kept in the same position. The reading was taken several times to be sure of the correct value. After ice had accumulated on the pipes, improving isolation, the nitrogen inlet temperature was about 79 K (exact values are given for each experiment). The flowrate was within the range of 15-25 m^3/h and more than 10 times the flowrate of the intermediate fluid. The flowrate differences will not largely affect the amount of heat transferred. A needle valve, or another valve capable of accurately controlling the flow rate, should be installed in the immediate vicinity of the tank outlet to improve flow rate control for future experiments on this system. The flow meter should also be investigated, to find the source of the reading fluctuations.

The IF is circulated by a pump. Upon changing the IF from propane to ethylene glycol and water the pump broke down and was replaced. Therefore the flowrate between the two experiments differ slightly: 1.16 m^3/h for propane and 1.26 m^3/h for glycol. The IF temperature is dependent on the temperature of water and nitrogen and reach a stable temperature after some time, typically a few degrees colder than water. The time of change is long, several hours, due to the large tank volume. The pressure is different for the two IFs: propane requires a high pressure to maintain liquid state and was pumped at about 7 barg, while glycol was pumped at about 1 barg. Again the exact values can be found in the recorded experimental data.

The water loop is controlled by the water heater/cooler machine. It allows the user to set a desired water temperature. The experiments were conducted at 10, 15 and 20°C. The flowrate was constant at 1.48 m^3/h. The water flowmeter had initial problems and it was found that the turbine was contaminated by rust and alien particles. It was cleaned, but the flowrate reading still showed incorrect values on a few occasions during the later experiments. It should be replaced if used in future experiments.

5.3 Data recording

Data are recorded after some time when all variables are stable, with special regard to temperatures. The data is then saved as an excel document with data from the last 400 seconds of the experiment, before a new water temperature is set and the experiments continue. For further information and details on the experiments refer to appendices one and two, for experiment description and laboratory log, respectively.

6.0 Ansys Fluent Simulations

Simulations of the regasification heat exchange is carried out using the Ansys FLUENT software for computational fluid dynamics. This involves several steps; building a geometry, generating a mesh grid, solving by iterative methods and finally analysing the results. These steps will be discussed in detail. The CFD analysis will be conducted on the propane-nitrogen heat exchanger, as this exchanger has higher temperature driving forces. Furthermore it is of higher interest because the purpose of the whole system is to increase the nitrogen temperature as much as possible.

6.1 Geometry

The geometry of the heat exchanger is simple and therefore the CFD geometry consists of few simplifications. The geometry of the heat exchanger is shown in figure 13. It is a simple counter-current tube in tube heat exchanger with only one, straight by-pass. Note that the flow of the outer pipe, which contains propane, enters the heat exchanger perpendicular to the water flow in the inner pipe.

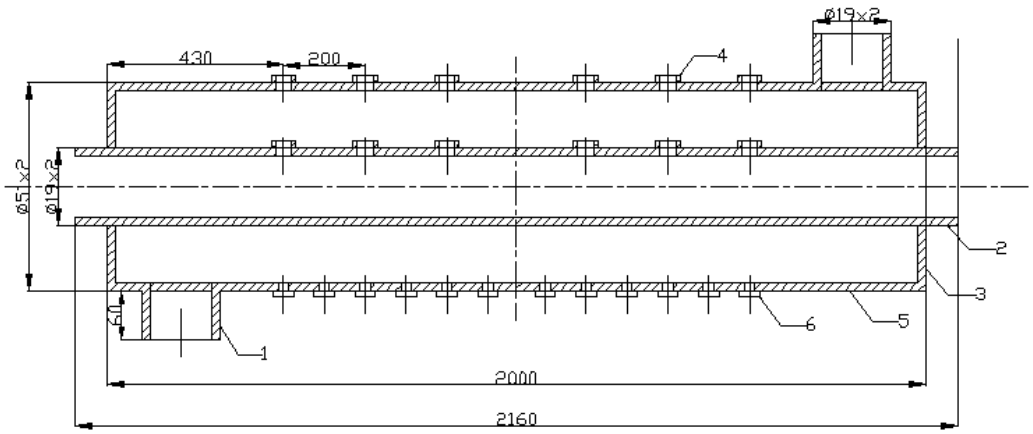

Figure 19: Heat exchanger dimensions

The relevant dimensions are given in figure 14.

Part	Size (mm)
The internal diameter of the inner pipe	15
The external diameter of the inner pipe	19
The internal diameter of the outer pipe	47
The external diameter of the outer pipe	51
The length of double-pipe	2000

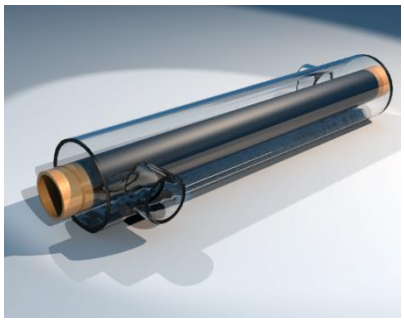

Figure 20: Heat exchanger dimensions and visualization (right picture)

The heat exchanger geometry is built using the Ansys Design Modeller. The propane inlet and outlet has been reduced to consist only of a face on the heat exchanger shell side. Furthermore the inner

pipe (tube) length is 2000 mm. The real system is 80 mm longer on each side. However, no heat exchange with the IF occurs in this area, so it is excluded from the model. The Cartesian origin is placed in the centre of the heat exchanger. The length of the heat exchanger is along the x-axis, measuring one metre in each direction, and the IF inlet is at the negative end of the x-axis.

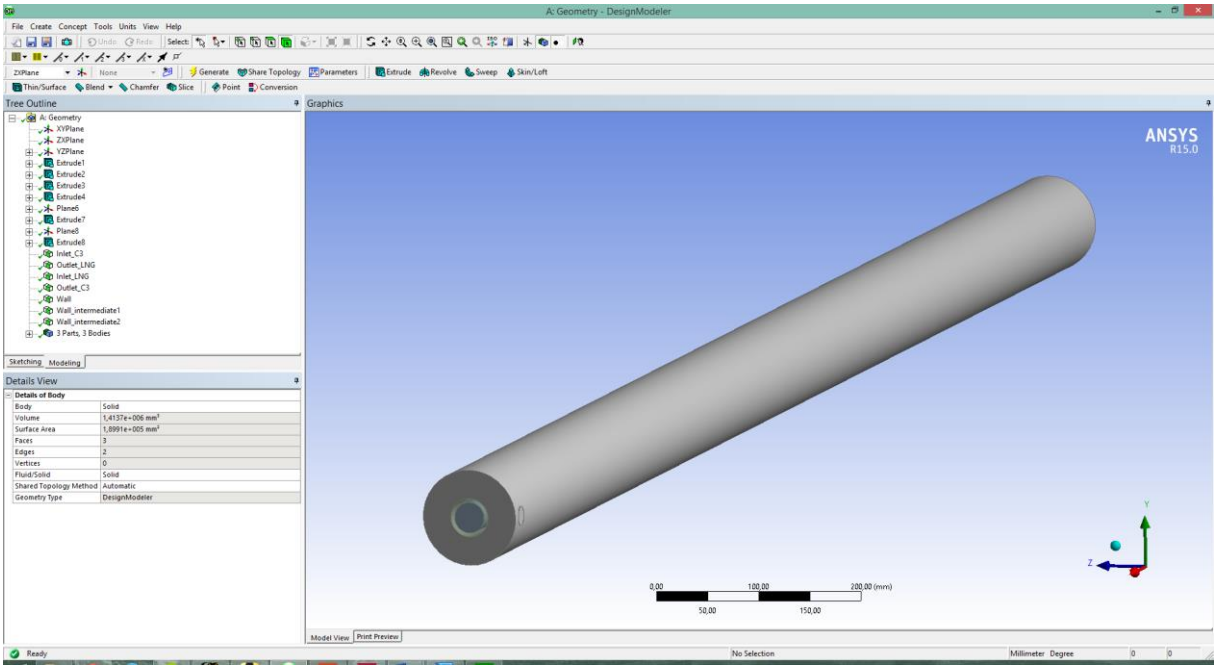

Figure 21: Simulation geometry

6.2 Mesh generation

The mesh is built using Ansys ICEM. Generally it is desirable to build a mesh with mainly hexahedral cells when working with simple geometries. In this case it may have been fitting to use tetra cells around the propane inlet and outlet to improve calculations in areas where the highest degree of turbulence is expected. Efforts to generate a hybrid mesh with tetra and hexa cells of sufficient quality has proved difficult and convergence was not reached with this type of mesh. Therefore only purely hexahedral meshes have been used. Two main, different types of meshes have been used: a mesh with a high degree of refinement near the wall and one without.

6.2.1 Mesh independence study

Obtaining a solution independent of the mesh density is important. If the solution changes with the density, it cannot be trusted. 2 different mesh grid types were developed, because different turbulence models require differently built mesh grids. The models that are combined with wall functions require a mesh without high near-wall density to avoid disturbance to the wall functions, while models that employ enhanced wall treatment require a high density near-wall grid with y+ values of about 1. The two will be referred to as non-refined and refined meshes, respectively. The non-refined solutions will be obtained from the realizable k-e model and the scalable wall functions, while the refined solutions will be obtained by the realizable k-e model with enhanced wall treatment.

Each of the mesh grid types were developed with different degrees of refinement, adding up to a total of 6 different mesh grids. The non-refined mesh has a coarse mesh of 196335 cells, a medium mesh of 365535 cells and a fine mesh of 624759 cells. The refined mesh has a coarse mesh of 192213 cells, a medium mesh of 454524 cells and a fine mesh of 735224 cells. It is generally agreed that the minimum orthogonal quality of the mesh should be higher than 0.3 in order to reach convergence. Using the “smooth mesh globally” tool it was possible to improve the quality of all meshes to a minimum of 0.3, some higher. This was later improved to above 0.4 in Fluent by using the command */mesh/repair-improve/improve-quality*. The refined mesh is displayed below.

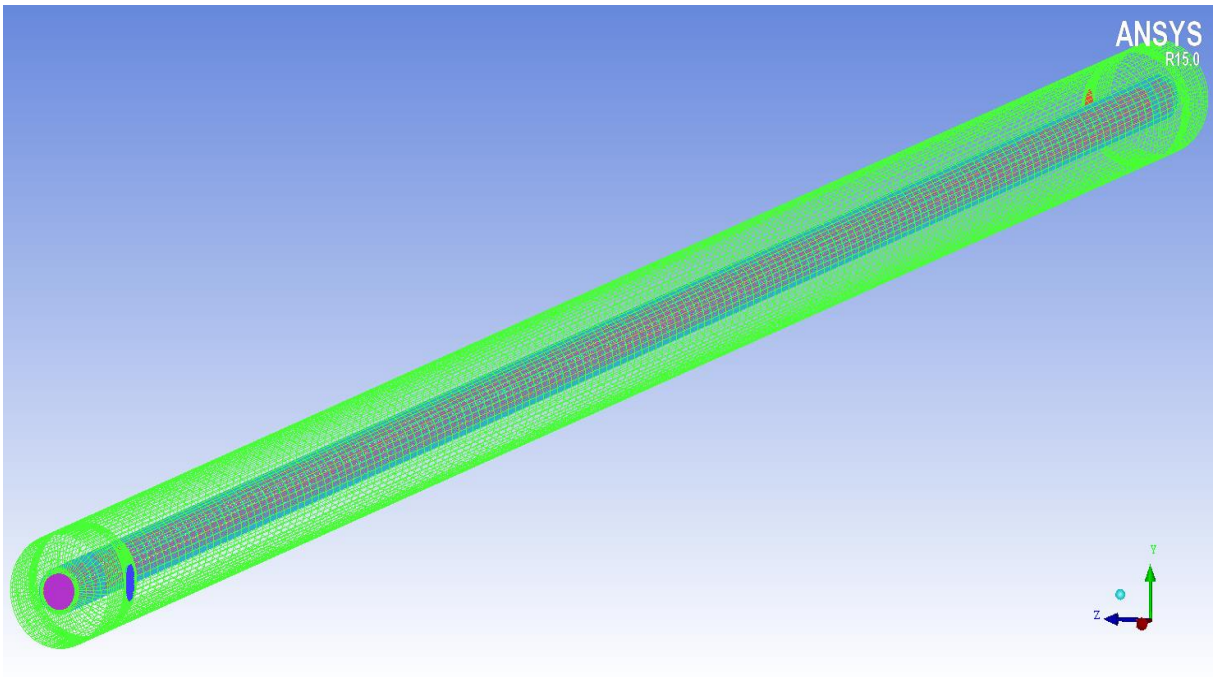

Figure 22: Hexahedral mesh

The grid independence study results are given in figure 23 and 24 as temperature along the x-direction. The temperature profiles are taken at the outer wall of the inner pipe, where the IF temperature undergoes the greatest changes. The non-refined mesh produced slightly different temperature profiles with the fine mesh differing from the coarse and medium meshes. This indicates that the fine mesh near-wall resolution is so high that the first node is within the wall function domain, i.e. the y+ values are too low. Furthermore the temperature is constant for about 50% of the heat exchanger length. The temperature profile is unlikely and the non-refined mesh grid is therefore discarded altogether. The refined mesh grids display better qualities; the profiles all have a decreasing temperature profile. The coarse mesh is somewhat different from the fine and medium meshes, indicating that the near-wall mesh resolution is too low. Subsequent simulations will continue with the medium mesh density, which is a good compromise between time-efficiency and accuracy.

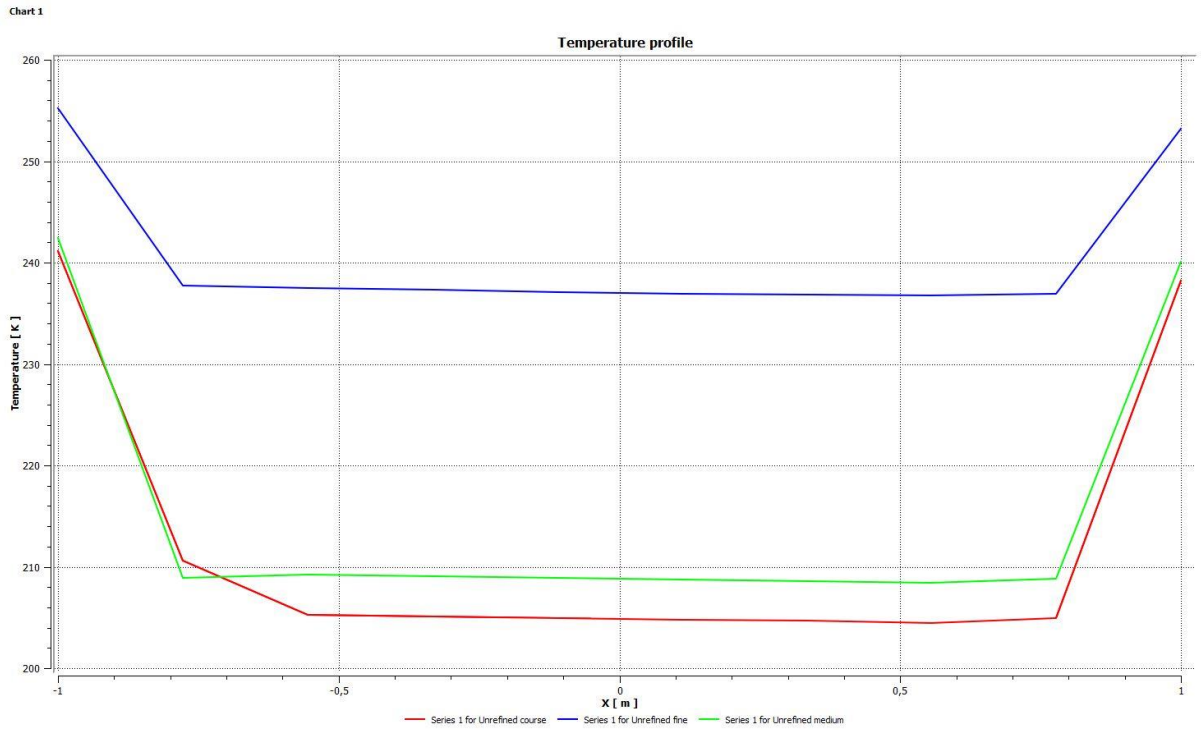

Figure 23: Hexahedral grid independence, non-refined

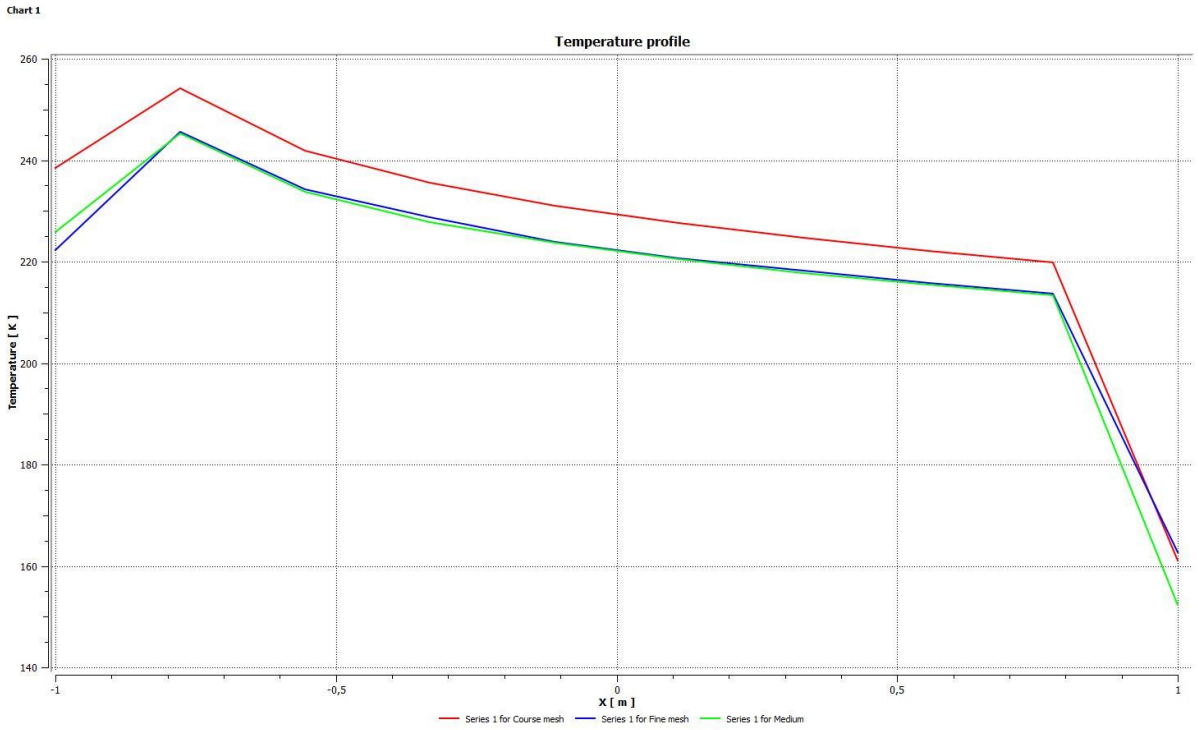

Figure 24: Hexahedral grid independence, refined

6.2.2 Y+ values

Y+ values play an important role in the selection of turbulence models and wall-treatment methods. As previously mentioned, the standard wall functions require high Y+ values, while the requirements for enhanced wall treatment, as can be used by $k-\varepsilon$, $k-\omega$ and other low-Reynolds number models, require low values. Y+ is a non-dimensional wall distance for a wall-bounded flow (CFD-wiki, 2015) and defined as in equation 4.1.

$$y^+ \equiv \frac{u_* y}{\nu} \tag{4.1}$$

u_* is the friction velocity, y is the distance to the wall and *v* is the kinematic viscosity. The requirements to y+ are summarized in figure 19.

Model	Y+ requirement	Simulation Y+ value
Standard wall functions	$30 < y^+ < 100$.	$10 < y^+$
Non-equilibrium wall functions	$30 < y^+ < 100$	$10 < y^+$
Enhanced wall treatment	$y^+ \leq 1$	$y^+ < 1$

Figure 25: Y+ values

As previously explained the unrefined meshes have all been discarded, leaving the refined meshes. These all have high mesh resolutions close to the wall across which the heat transfer between the two fluids occur. The y+ values of the meshes are all less than 1, which allows for the use of enhanced wall treatment.

6.3 Solution

6.3.1 Boundary conditions

The simulations are used as a verification of the experiments and vice versa. Furthermore the simulations are used to clearly compare the different experiments. As explained in chapter 5 it was troublesome to conduct experiments for exactly equal boundary conditions every time. With simulations, however, this is no problem. The boundary conditions for the simulations are set as close to the real values as possible and are summarized in figure 26. Note that because of the troubles of maintaining a constant mass flow for nitrogen, the mass flow has been calculated by equations 2.1-2.3 and no heat loss throughout the heat exchanger is assumed. To fulfill the calculation the heat capacities were assumed constant and found at 288K and 79K for propane and nitrogen, respectively. The temperature differences between inlets and outlets were similar in all experiments and dependent on the water inlet temperatures. The IF inlet temperatures are listed in the table below.

Type	Variable	Outer (IF) tube	Inner (N2) tube
Mass flow - inlet	Mass flow	0.1643 kg/s	0.28 kg/s
	Temperature	Subject to water temperatures:	79 K
	$T_{water} = 20^{\circ}C$	288.9 K	
	$T_{water} = 15^{\circ}C$	285.7 K	
	$T_{water} = 10^{\circ}C$	281.4 K	
	Pressure (C3)	7.5 bara	1.5 bara
	Pressure (glycol)	1.5 bara	1.5 bara
Outlet - vent	-	-	-
Wall	No slip condition	No heat flux	Coupled
Turbulence	Intensity	10%	10%

Figure 26: Simulation boundary conditions

6.3.2 Discretization scheme

Every model is solved initially with the first order upwind scheme. When the model converges the scheme is changed to the second order to achieve a higher degree of accuracy. The first order scheme may increase the numerical discretization error when the flow is not aligned with the mesh (Ansys FLUENT user guide, 2015). This is indeed the case in this project, where the propane flow enters and exits the heat exchanger perpendicular to the hexahedral mesh. In tetra meshes the flow is never aligned with the mesh. Generally it can be said that the first order discretization yields better convergence, though somewhat at the expense of accuracy. (Ansys FLUENT user guide, 2015). Therefore the second order is used after an initial solution is found.

6.3.3 Measure of convergence

Observation of convergence in Ansys FLUENT is complicated and subject to several different criteria. If the criteria are made strict the simulation time increases. In this model convergence is taken to be when:

- The solution no longer changes with subsequent iterations
- Overall mass, momentum, energy and scalar balances are achieved
- A decrease in solution residuals by an order of 10-3
- The scaled energy residual decreases to an order of 10-6
- Scaled species residuals decreases to an order of 10-4

Surface monitors are set up to confirm that the converged solution is correct, i.e. a mass-averaged monitor for temperature at each of the outlets. The monitors are used to calculate the total heat transfer as well as control the solution. By using both first and second order discretization schemes as described above, convergence was reached for all simulations by the criteria presented above, usually after some 300 iterations. The simulation results are presented in the next chapter.

7.0 Results

This chapter will outline the results of the experiments and simulations and compare the heat transfer properties of the two intermediate fluids. The simulations are used to a great extent in the comparative analysis, as simulations are able to provide exactly equal boundary conditions for the different cases and fluids.

7.1 Simulation reliability control

To control that the simulations are reliable they are compared to the experiments. In this process a simulation is calculated for the exact same boundary conditions as recorded in an experiment. For this purpose experiment number 3, propane with water at 20°C, is chosen. It is one of the most stable and reliable experiments. The simulation is carried out with two different turbulence models, the realizable $k-\varepsilon$ model and the SST $k-\omega$ model, to see which model that best fit the experiments. The result of the study is shown in figure 27. As seen both simulation models are well within the uncertainty of the experimental data. The realizable $k-\varepsilon$ model fit better than the SST $k-\omega$ model, and will be used for the subsequent simulations.

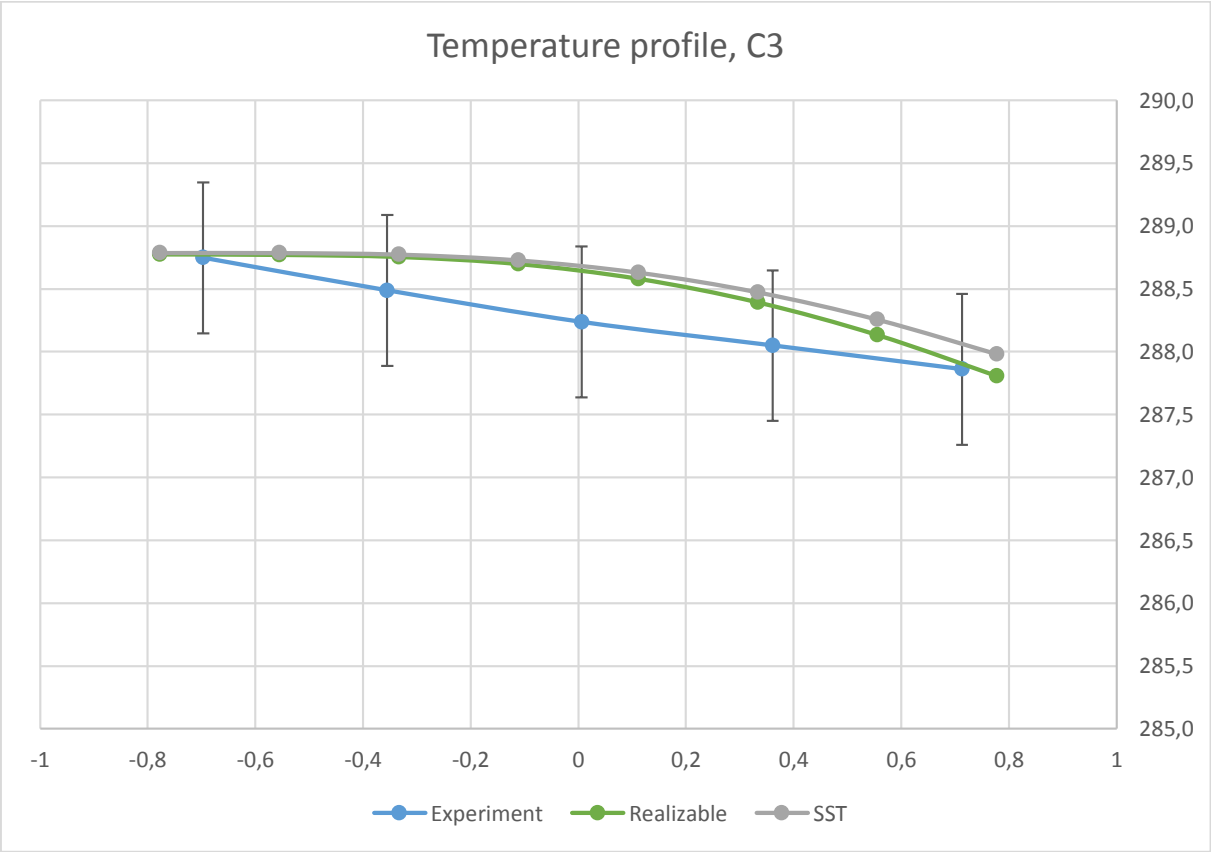

Figure 27: C3 simulation temperature profile

There is an observable difference between simulation and experiment temperatures at the middle region of the heat exchanger. This may be attributed to flow disturbance by the sensors heads, which are installed some 10 mm into the flow. The temperatures are close to equal at the inlet and outlet. Furthermore the recorded outlet temperatures equal: 287.6 K for propane at the heat exchanger outlet and 287.6 K for the simulations, calculated by mass-average. For nitrogen the outlet temperature is higher in the simulations, 83.2 K compared to 79.6 K for the experiments. The difference is attributed to the non-changing temperature profile of the straight tube in which nitrogen flows. The sensor will record only one point in the profile, while the simulations calculate the higher mass-averaged temperature. For the intermediate fluid the sensor reading will be more correct due to the perpendicular orientation of the inlet and outlet pipes, which causes turbulent mixing of the fluid prior to exiting the heat exchanger. The simulations for glycol as IF also display accuracy, as seen in figure 28 below (note that the second last sensor had some difficulties during the experiment). Overall the simulations are deemed accurate.

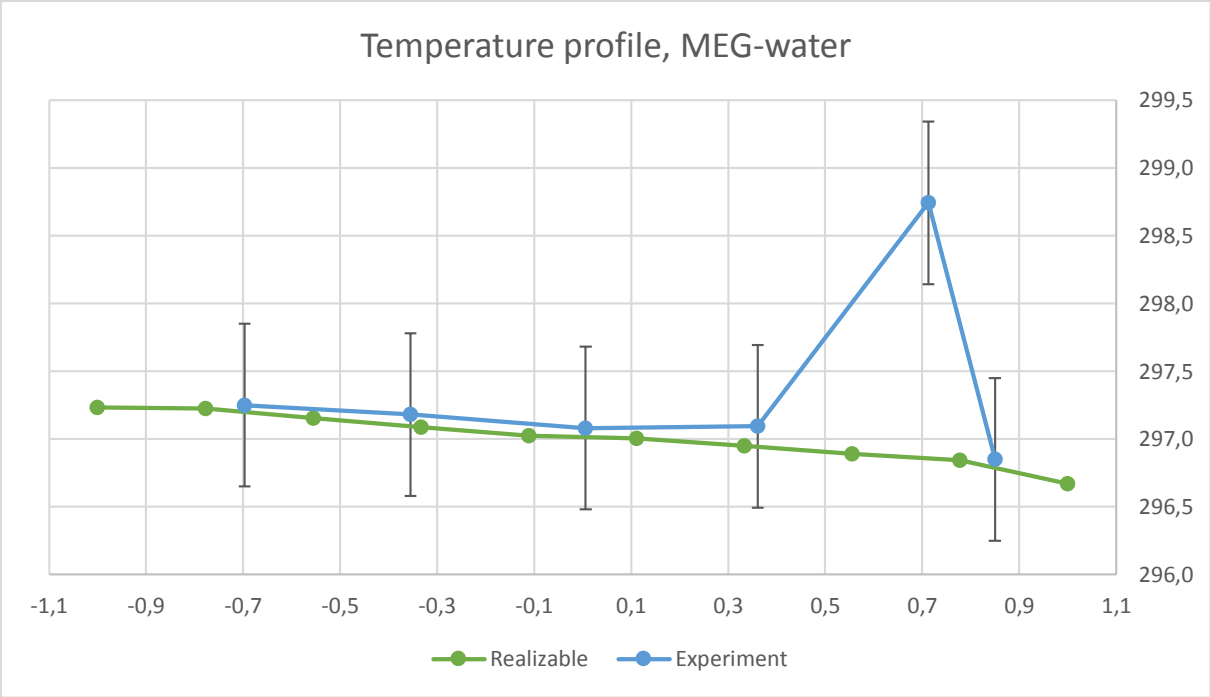

Figure 28: Glycol simulation temperature profile

To further control the reliability of the simulations a calculation of relevant dimensionless parameters is carries out, for the nitrogen side of the heat exchanger. Theoretical values for Reynolds, Prandtl and Nusselt numbers are found by equations 2.8 through 2.10. The result is given below and the values of the relevant variables are found through REFPROP, equal to those of the simulations.

$$\mathrm{Pr} = \frac{c_p \mu}{k} = 0.84 \qquad \mathrm{Re} = \frac{\rho U L}{\mu} = 1538 \qquad Nu_L = 0.023\,\mathrm{Re}^{0.8}\,\mathrm{Pr}^{0.4} = 7.62$$

The dimensionless number values are as expected; Prandtl lies in the gas range from 0.7-1.0 and is above the limit (0.6) that approves the use of equation 2.8. The Nusselt number for flows in circular pipes with constant surface heat flux is 4.36 (Incropera et. al., 2006). Here, the heat flux is not constant and the flow is turbulent in some areas, which leaves a slightly higher Nusselt number value. The calculation of Nusselt number in FLUENT is carried out by finding the local Nusselt numbers by the following formula:

$$Nu = \frac{q_p X_p}{(T_w - T_b)k} \tag{7.1}$$

The subscript p denotes the point at which the calculation is done, w is for wall and b is for bulk, denoting the wall and fluid bulk temperature, respectively. Prior to this calculation iso-surfaces and points were set up in FLUENT to find the wall temperature, bulk fluid temperature and local heat flux. The result of the calculation is given below. Note that the coordinate origin was shifted to the end of the pipe for this calculation, so as to avoid negative Nusselt numbers.

X_p [m]	q_p [W/m^2]	T_w [K]	T_b [K]	Nu
0	107.15	100.92	212.26	0.00
0.3	5954.63	100.62	222.06	2.00
0.65	5510.87	98.67	212.08	4.30
0.9	5348.95	97.73	208.25	5.93
1.1	5252.83	96.96	205.44	7.26
1.35	5158.72	96.18	202.90	8.89
1.7	5126.79	94.79	199.02	11.39
2	923.23	79.71	90.04	24.35

Figure 29: Nusselt number calculation for FLUENT

The average Nusselt number is 8.02, by the Ansys FLUENT calculation. By comparison the theoretical value is 7.62 and the deviation between the two is 0.4. The deviation is small enough for the simulations to be supported by the theoretical calculation. X_p increases along the direction of propane flow, and against that of nitrogen. Note how the heat flux decreases along the x-direction (with the exception of the very ends of the heat exchanger). As the temperature profile and boundary layer is established, and the flow becomes laminar, the heat flux decreases. The decrease in heat flux could be mitigated by creating more turbulence along the heat exchanger.

7.2 Experimental results

Experiments with propane and glycol as intermediate fluids were carried out to conclusion. For details on the progress throughout the experiments refer to appendix 2. From both experiments and simulations it is observed that the temperature difference from inlet to outlet for all fluids is low; the heat transfer area of the tube-in-tube heat exchanger is too low to produce a significant and effective heat transfer. The fluids may be compared, though the error (+- 0.6K) is high relative to the temperature differences. The recorded temperatures for experiment no. 3 is given in figure 29. The two high values are water outlet and inlet from left to right, and the rest are propane temperatures along the direction of flow. The left group show propane temperatures increasing against seawater, while the right group show propane temperatures decreasing against nitrogen. The nitrogen temperatures are not displayed as they are too low. The temperature difference between the first and last (inlet and outlet) points for propane are different: the temperature is increasing as the fluid circulates to the tank and is pumped back into the system. Most likely the pump adds the heat, though some might also come from heat in-leak from the surroundings.

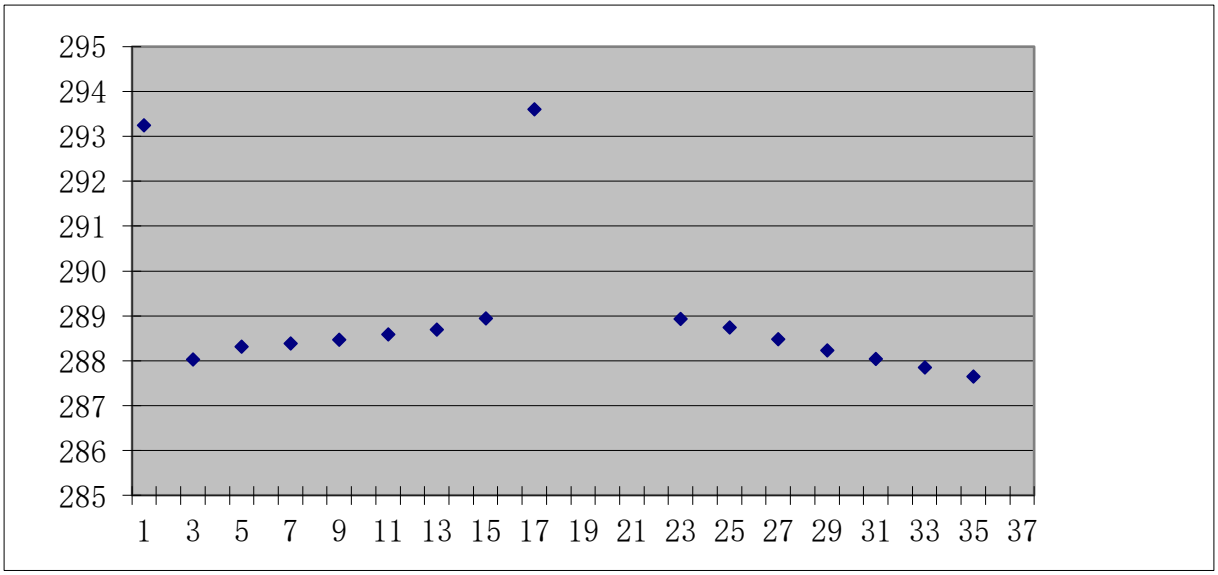

Figure 30: Experimental result, C3, water at 20 degrees C

The first and only experiment recorded with glycol is shown below in figure 31. A major fault occurred during the experiments: after changing the IF from propane to glycol the circulation pump broke down. It was quickly replaced by a pump with similar operating properties. However, it was found that the new pump added much more heat to the liquid during operation. The pump heat increased the temperature of the IF to such a degree that when a steady state was reached, both water and nitrogen was cooling the IF. Due to this condition the glycol experiments cannot be directly compared to the propane experiments. Instead simulations will be used for the comparison, validated by the experiments as is done in chapter 6.1. Simulations have a great advantage in the

ability to produce exactly equal boundary conditions for each different experiment, which will clarify and detail the differences between the two intermediate fluids.

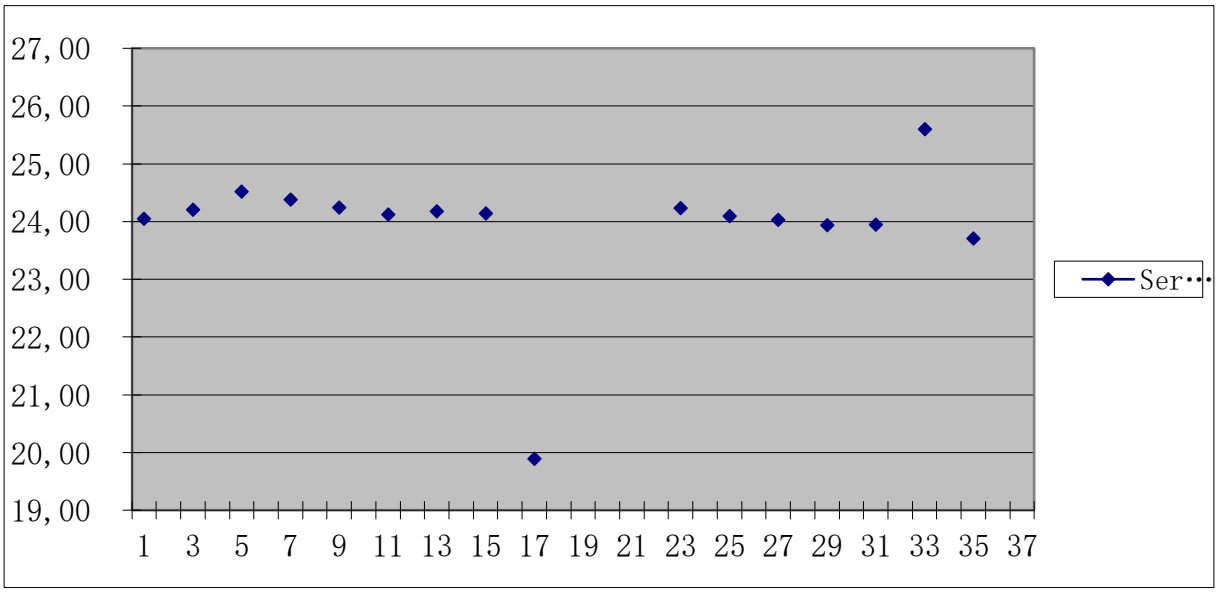

Figure 31: Experimental result, glycol, water at 20 degrees C

7.3 Simulation results

Six experiments are carried out to compare the two IFs, three for each at 20, 15 and 10°C. During the simulations the mass-averaged temperatures are recorded at both fluid outlets. Then, from equation 2.1, the heat transferred from the IFs is calculated. A comparison of the total heat transfer of the six simulations is depicted in figure 32.

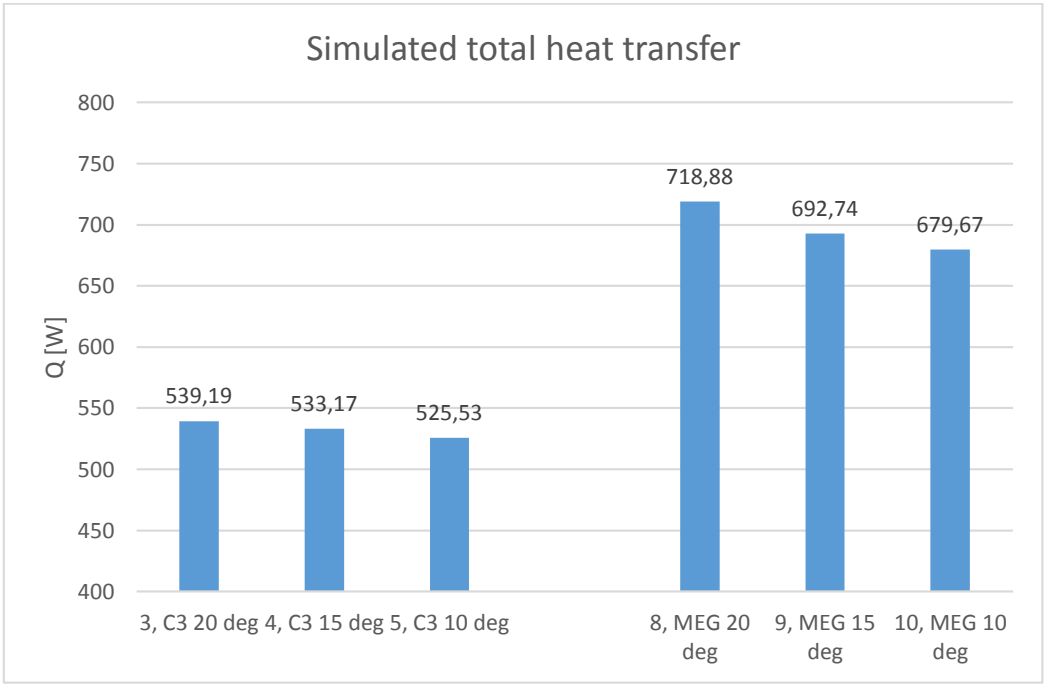

Figure 32: Simulation result, total heat transfer

7.4 Discussion

As seen in figure 32 the heat transfer is decreasing with decreasing water temperature, as is expected due to decreasing temperature driving forces. Furthermore the glycol mixture displays significantly more heat transferred, which is also expected as the specific heat capacity is much larger. Note also that the heat transfer is small: less than a kilowatt. The heat transfer area is too small to obtain any larger temperature difference or heat transfer.

In an industrial scale plant LNG vaporizes against the intermediate fluid and the temperature is further increased to about -40℃, as suggested by Kobe Steel, ltd. (an increase of 120 degrees or more). The configuration places strain on the intermediate fluid. To fulfil the heating target the IF temperature must decrease substantially, and flow rate and heat transfer area must be high. On the heat source (water) side, the temperature drop is limited to some 5.5℃ (Japan, Kobe Steel ltd.) due to environmental concerns.

Propane and glycol have different characteristics. The freezing point of the glycol-water mixture was calculated to -33℃ at ambient pressure by interpolating tables from engineeringtoolbox.com, while the freezing point of propane is -187.8℃. The temperature of propane can therefore be allowed to decrease significantly more than the glycol mixture. However, as seen in the experiments and simulations the specific heat of glycol is significantly higher than propane, and glycol will require less heat transfer area to transfer the same amount of heat. Furthermore, glycol does not significantly expand during freezing and will not burst the system in which it flows, another advantage. Still, the temperature of glycol cannot be allowed to drop to near freezing point levels which restricts the use.

In the LNG regasification configuration most commonly employed, amongst other by Hamworthy Gas Systems (today owned by Wärtsilä) (2010), the propane condenses and evaporates throughout the loop. By using the latent heat of vaporization of propane for regasification of LNG the temperature drop is only some 20-30 degrees. This configuration is not possible with glycol. Utilizing the latent heat transfer for propane will also reduce the required heat transfer surface area. Using propane requires careful design with regard to flammability and explosion. Glycol is the safer choice in this regard.

Hamworthy (2010) have also supplied a system using glycol, though steam is used as heat source. 2.5% of the LNG is used to produce steam in this configuration, increasing operational costs. The steam heats the glycol to 90℃, and the glycol temperature is reduced to 30℃ in the LNG heat exchanger. The higher temperatures reduce the risk of freezing.

Consider 3 MMTPA LNG which is vaporized and heated from -160 to −40℃. The LNG latent heat of vaporization is 500 kJ/kg and C_p og natural gas is taken to be 2.34 kJ/kg K (www.engineeringtoolbox.com, 2015). The total heat required is

$$Q = \dot{m}c_p(T_{in} - T_{out}) + \dot{m}L_v = 95.13\frac{kg}{s} \cdot 2.34\frac{kJ}{kgK} \cdot 120K + 95.13\frac{kg}{s} \cdot 500\frac{kJ}{kg} = 74.27MW$$

The heating requirement for LNG is high. The IF fluid is set to enter at 10℃ and exit at -20℃, and the LMTD is then calculated to 87.4 degrees. The heating requirement of LNG in the laboratory scale, that is with a flow rate of 0.28 kg/s, is much smaller. By the same equation used above the heating requirement would be 218.6 kW. In a preliminary project report to this thesis, based on a master thesis experiment at SJTU by Ji Xin (2014), the overall heat transfer coefficient of the laboratory rig was calculated to 250 W/m^{2}K . To achieve 218.k kW in the laboratory, the required heat transfer area is 10 m^2. This would be possible to supply if the tube-in-tube heat exchanger is converted to a shell and tube. With tubes of the same diameter (inner diameter 15mm) and for example 25 tubes each 8.5 meters long. The dimensions are quite stretched, with an length increase from 2 to 8.5 meters. Some may argue that the heat exchanger is too long for the laboratory scale. On an industrial scale the area is more feasible. Xu et. al. (2015) calculated an U for propane at about 600 W/m^{2}K, which by these calculations would require an evaporator area of about 1400 m^2. Xu et. al. (2015) calculate the total area (evaporator and condenser) to slightly less than 3000 m^2. This indicates that both IFs investigated in this thesis are feasible for use in an IFV. However, in the case of propane the results suggest that the evaporating-condensing configuration is better due to decreased heat transfer area.

The overall heat transfer coefficient should be increased, by augmenting a shell and tube heat exchanger or choosing another type of heat exchanger. Liu et. al. (2013) showed that spiral-wound heat exchangers can provide a compact solution, with 200 m^2/m^3, and Hamworthy (2010) has delivered regasification systems using printed circuit heat exchangers. If propane is used, allowing IF vaporization and condensation would reduce the heat transfer area. Glycol cannot be used in this configuration, though using glycol would still reduce the surface area due to the higher heat capacity. Some of the heat load can also be left to the trim heater, where evaporated gas is heated directly by seawater. The heat transfer area calculations are summarized in the table below.

	Unit	Laboratory scale	Industrial scale
Flowrate	kg/s	0.28	95.13
Heat, Q	kW	218.6	74 270
LMTD	K	87.411	87.411
UA	kW/K	2.500	849.644
Surface area	m^2	10	< 3000
U	W/m^2K	250	600

Figure 33: Summary of heat transfer surface area calculations

8.0 Conclusion

This work has compared propane and glycol as heat transfer fluids in an intermediate fluid vaporizer. It is found that glycol has a greater capacity for heat transfer than propane. However, glycol is limited by a freezing point at -33℃. It is the safer option due to it being non-flammable and non-explosive, and it will not expand and burst pipes if freezing occurs.

Most importantly, it is found that the heat transfer surface area of the current configuration is too small. The tube-in-tube heat exchanger that was built in the laboratory is thought to be part of a tube bundle in a shell and tube heat exchanger, but still the surface area is small when considering the required heat transfer of LNG regasification. Industrial plants with propane in operation today use a evaporating-condensing configuration, which reduce the surface area requirement. The current configuration with no phase change of propane may be possible, but is not recommended as it would be inefficient when compared to other options. Heat transfer area calculations indicate that the requirements would be similar to results established by other researchers, such as Xu et. al. (2015) and Pu et. al. (2014). The calculations also indicate that the evaporating-condensing configuration is a better choice for propane, as it reduces both heat transfer area and temperature difference. When compared to glycol, propane is inferior in the non-phase changing condition even with the lower freezing point.

Glycol can possibly be used in the current configuration, as it displays better heat transfer properties than propane and has a notably higher heat capacity. Still, further research is needed to determine the heat transfer configuration for glycol.

8.1 Recommendation for further work

Further work is definitely required before a complete LNG vaporizer design based on this research is possible. Most importantly experiments should be made with heat exchangers with more area. It is important to investigate the heat transfer characteristics of the intermediate fluids in cases with realistic temperature differences, even when the experiment would be scaled to a laboratory.

In the endeavour to achieve realistic temperature differences in the laboratory, the heat transfer surface area should be increased. The efficient solution would be to build a shell and tube heat exchanger, instead of the single tube-in-tube heat exchanger, in laboratory-scale. This could possibly better allow for a evaporating-condensing configuration of the IF. Other heat exchanger types may also be considered, such as printed circuit heat exchangers, plate-plate heat exchanger or spiral-

wound heat exchangers. In any case it is strongly recommended to calculate and predict heat transfer area, temperatures and other parameters prior to actually building a test rig.

In the case where larger surface area experiments are infeasible for laboratory work it is recommended that CFD is used to investigate both industrial and laboratory scale heat exchange for different heat exchanger configurations. In the case of full-scale simulations the use of symmetry planes and investigation of interesting areas of the heat exchanger only would decrease computational time, which would be crucial. CFD is a powerful tool to visualize and investigate heat and fluid dynamics, especially when real-life experiments are difficult to conduct.

References

[1] WANG XY, LUO YX, LONG G, ZHOU ZB. (2006) Research on China's natural gas supply security strategy. *China Energy Resources*, 28 (2) p. 23–25

[2] GREAT BRITAIN. BRITISH PETROLEUM (BP)(2014). *Statistical Review of World Energy*

[3] UNITED STATES OF AMERICA. US ENERGY INFORMATION ADMINISTRATION. (2014): *Today in Energy*. [Online] Available from: www.eia.gov/todayinenergy/detail.cfm?id=17591. [Accessed 8th February 2015]

[4] UNITED STATES OF AMERICA. US ENERGY INFORMATION ADMINISTRATION. (2014) *China.* [Online] Available from: www.eia.gov/countries/cab.cfm?fips=CH. [Accessed 4th February 2015]

[5] PATEL D, MAK J, RIVERA D, ANGTUACO J. (2013) LNG vaporizer selection based on site ambient conditions. *The 17th International conference & exhibition on LNG (LNG 17), Houston, Texas.* [Online] Available from: www.gastechnology.org/training/documents/lng17-proceedings/materials-4-dhirav_patel.pdf [Accessed 2nd July 2015]

[6] XU SQ, CHENG Q, ZHUANG LJ, TANG B, REN QJ, ZHANG XJ (2015) LNG vaporizers using various refrigerants as intermediate fluid: comparison of the required area. *Journal of Natural Gas Science and Engineering* [Online] 25 p.1-9 Available from: www.sciencedirect.com [Accessed 5th July 2015]

[7] PU L, QU ZG, BAI YH, QI D, SONG K, YI P (2014) Thermal performance analysis of intermediate fluid vaporizer for liquefied natural gas. *Applied thermal engineering.* [Online] 65 p.564-574 Available from: www.sciencedirect.com [Accessed 5th July 2015]

[8] LIU FX, DAI YQ, WEI W (2013) Feasibility of intermediate fluid vaporizer with spiral wound tubes. *China Petroleum Processing and Petrochemical Technology*. 15(1) p.73-77.

[9] GREAT BRITAIN. HAMWORTHY (2010) Intermediate fluid vaporizers for LNG Re-gasification vessels, SRV's and FSRU's. *Offshore technology conference 20809* [Online] Available from: www.onepetro.org/download/conference-paper/OTC-20809-MS?id=conference-paper%2FOTC-20809-MS [Accessed 2nd July 2015]

[10] GREAT BRITAIN. FOSTER WHEELER (2012). *LNG terminal cold energy integration opportunities offered by contractors*. [Online] Available at www.fwc.com/getmedia/aa4355b7-e24b-40fe-9b3c-99359af7b148/LNG-Journal-Mar12-p22-24.pdf.aspx?ext=.pdf [Accessed 04.02.2014]

[11] SZARGUT J & SZCZYGIEL I (2009) Utilization of the cryogenic exergy of LNG for the production of electricity. *Energy* [Online] 34 p.827-837. Available from: www.sciencedirect.com [Accessed 5th July 2015]

[12]LIU YN, GUO KH (2011) A novel cryogenic power cycle for LNG cold energy recovery. *Energy* [Online] 36 (5) p.2828-2833. Available from: www.sciencedirect.com [Accessed 15th May 2015]

[13]LIN WS, ZHANG N, GU AZ. (2010) LNG: A necessary part in China's future energy infrastructure. *Energy* [Online] 35 (11) p.4383-4391. Available from: www.sciencedirect.com [Accessed 3rd July 2015]

[14]Email correspondence with Prof. Lin Wensheng, linwsh@sjtu.edu.cn

[15]INCROPERA F. P. et. al. (2006) *Fundamentals of Heat and Mass Transfer*. 6th edition. Wiley.

[16] ANDRSSON B et. al. (2011) *Computational Fluid Dynamics for Chemical Engineers*. 6th edition. Cambridge.

[17] ANSYS FLUENT (2015) *User* guide [Online] Available from: www.ansys.com [Accessed 8th May 2015]

[18] CFD-WIKI. (2015) [Online] Available from: www.cfd-online.com/Wiki/. [Accessed 8th May 2015]

[19] JAPAN. KOBE STEEL LDT. (2005) *Overview of ORV and IFV characteristics and operation in LNG receiving terminals in Japan and worldwide.* Available from: www.lngexpress.com/rcp/presentations/MasaoEndo110905.pdf. [Accessed 2nd July 2015]

[20] THE ENGINEERING TOOLBOX (2015) *Ethylene glycol heat-transfer fluid.* [Online] Available from: www.engineeringtoolbox.com/ethylene-glycol-d_146.html. [Accessed 2nd July 2015]

[21]SOLBERG E. (2015) Project report: LNG regasification system with propane intermediate fluid vaporizer. *Norwegian University of Science and Technology*. Based on experimental results from a master thesis by Ji Xin (2015)

List of figures

Appendix 1: Experimental setup

A1.1 Background and purpose

The purpose of the experiment is to study the heat transfer in an IFV LNG regasification system and compare the performance of different intermediate fluids. The properties of propane and mono-ethylene glycol in a water mix as intermediate fluid between LNG and water shall be investigated. For safety reasons nitrogen will be used in place of LNG. The experiments will be carried out with constant mass flows, for which temperatures will be monitored. Thereafter the overall heat transfer will be compared.

LNG terminals are usually found on the shore or at sea in FSRUs. The system will be studied at different water temperatures. Different mixtures of water and glycol will also be investigated.

The goal is ultimately to analyse the heat transfer in order to obtain a theoretical basis for design and calculation of an IFV.

A1.2 Experimental setup

The process flow chart of the experiment is shown in figure A.1. This experimental system consists of an IF, a heat source seawater circuit and a cold source LN2 circuit. The liquid nitrogen is vaporized during heat transfer with the IF in the N2-C3 heat exchanger. The IF is cooled by the nitrogen and returned to the tank. From the tank IF is pumped first to be heated with seawater before entering the nitrogen heat exchanger. Seawater is supplied at the desired temperature by electric heating of the closed circuit. LN2 exits the heat exchanger and is vented to air. The flow of all fluids is adjustable and measured by flowmeters. Nitrogen (LN2) was used instead of LNG for safety, as well as easy acquisition of materials.

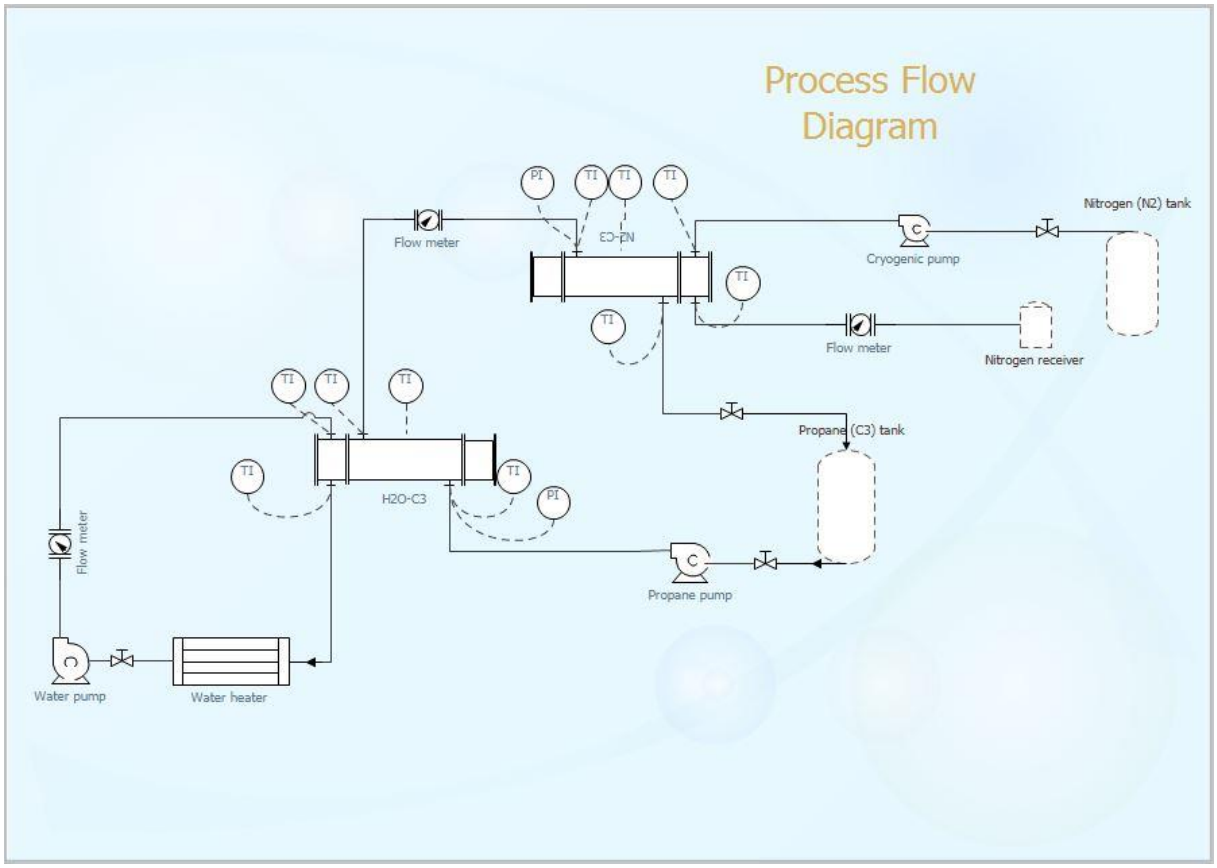

Figure A1: The heat transfer experiment process flow chart

A1.3 Experimental test section

Both heat exchangers are simple tube in tube heat exchangers. The main structure is shown in figure A2. Note that in this experiment thermocouple sensors (4) are only installed in the outer pipe section only, as well as all inlets and outlets.

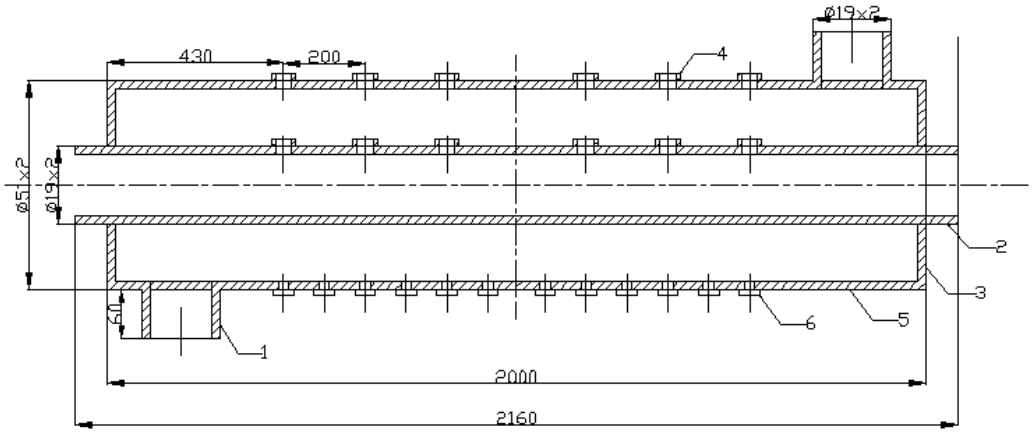

Figure A2: The heat exchanger dimensions

1	Inlet and outlet of propane
2	Water pipeline
3	Propane Pipeline
4	Thermocouples
5	Outer pipe wall
6	Thermocouple wire bundle outlet

The inner and outer tube are both smooth pipes. For both heat exchangers the IF flows in the outer tube. The length of heat transfer section is 2000mm. Figure A3 shows the detailed size of pipes.

	Size [mm]
The internal diameter of the inner pipe	15
The external diameter of the inner pipe	19
The internal diameter of the outer pipe	47
The external diameter of the outer pipe	51
The length of double-pipe	2000
Distance from edge to IF inlet/outlet	90

Figure A3: Relevant dimensions

The positions of the thermocouple sensors along the x-axis (length of the heat exchangers) are given below. There are five thermocouples in the outer tube side, as well as one thermocouple in each inlet and outlet, in total 18.

Test section	x-coordinate [mm]
1	303
2	655
3	1016
4	1367
5	1671

Table 1 Sensor position

A1.4 Experimental measurement parameters and measurement apparatus

A1.4.1 Measurement variables

1. Mass flow of IF, water and nitrogen
2. Pressure of IF at the heat exchanger inlets
3. Inlet and outlet temperature of IF, water and nitrogen
4. Temperature of IF at 5 locations along the heat exchangers
5. Water tank temperature

A1.4.2 Measurement apparatus

Mass flow

Rotameters are used to measure the mass flows. Installation is done after thorough cleaning of all pipes. The rotameters are controlled by hand valves.

Temperature

The temperatures are measured in order to obtain the overall heat transfer of the system. The thermocouple sensors are all of the type PT-100. The accuracy is +- 0.1 K.

The water temperature is measured by a thermometer installed in the water tank.

IF inlet pressure

The pressure is monitored at the inlet of the heat exchangers to ensure that propane is in its liquid state. The pressure of the other fluids is assumed to be at ambient levels.

A1.5 Experiment method

Experiment preparation

In advance of the experiment the following will be addressed: assigning test points, checking air tightness and vacuum pumping the pipes.

Temperature test points are set up at the inlet and outlet and every cross section segment. Pressure test points are set up at the outer pipe, and mass flux at the inlets. The thermocouples, pressure transmitter and power acquisition equipment is tested and calibrated in advance of the experiments.

After installation the system tightness is tested by filling the system with nitrogen, and humidifying all bonding points and connections by soap water. If any soap bubbles can be observed by eye the tightness is insufficient and the connection is checked and tightened. The system is subsequently kept pressurized for at least 48 hours to ensure tightness; if the pressure drop is below 20 kPa the tightness is deemed sufficient.

The system is vacuum pumped to ensure that no gas is present. The system is pumped to -0.1 MPa gauge pressure, after which liquid propane is poured in to the system until it reaches 0 MPa gauge pressure. This process is repeated 3 times.

Experiment procedure:

1. Check all system valves. All valves should be in the correct position, open or closed according to the experimental conditions
2. Start the Keithley multimeter and the computer
3. Turn on the water heater unit
4. Choose the water temperature according to the experiment demand
5. Open the water cycle valve slowly until the water flow rate reaches the desired flow rate
6. Control the water temperature by second means: place a mercury-in-glass thermometer into the water tank. Control that the temperature is the same as is read from the water unit display.
7. Open the propane tank inlet and outlet valves (outdoors, white valves)
8. Connect the nitrogen cycle pipe to the nitrogen tank. Open the nitrogen tank valves. Wait until the nitrogen temperature and flowrate are both stable (ice will form on the pipes, increasing isolation)

9. Ensure that the propane is liquid for the temperature and pressure conditions. Increase the propane flowrate to the pre-set rate. Observe temperature stabilization.
10. Increase the nitrogen flowrate to the desired value.
11. Continuously monitor the changes in temperature and pressure.
12. Monitor until pressure and inlet/outlet temperatures equal the theoretical value
13. Ensure that the system operation is at a steady state at the desired conditions
14. When all sensors are stable, record the data on the computer
15. Adjust parameters according to the need. For this experiment the water temperatures will be changed. Repeat steps 11-14.
16. When the experiment has ended, close the nitrogen vales. The nitrogen will exit the system.
17. Close the propane inlet valve. Let the propane flow back to the tank. Stop the propane pump.
18. Close the water valves and turn off the water heater
19. Shut down all systems

A1.6 Boundary conditions

The nitrogen (氮) loop:

The nitrogen will be drawn from a tank as saturated liquid. Direct scaling of from industrial to experimental size is difficult because an industrial size heat exchanger would contain more than one pipe. Practicality indicates that the mass flow of nitrogen should be in the order of 0.1 kg/s. The mass flow of nitrogen should correspond to the vaporization of 1 kg of LNG per second. The latent heat of vaporization ratio LNG / N2 is about 2.6 (an estimated 511,72 kJ/kg of LNG against 199 kJ/kg for Nitrogen). Therefore the suggested mass flow of nitrogen is 0.26 kg/s, or in terms of volume per time 0.321 l/s.

The heat exchanger volume (inner tube side) is π·0.015 $\pi \cdot (0.015^2 / 4) \cdot 2 = 1.414$ litres and sufficient for the desired mass flow. As the diameter of the inlet is 15 mm the flow velocity is 8 m/s.

The intermediate fluid (丙烷还乙二醇) loop:

The intermediate fluid (IF) will be propane and a water-glycol mix in different experiments. The mass flow of the IF will be set to completely vaporize the nitrogen, as a minimum, though it is desirable to reach as high a temperature as possible. For nitrogen to reach a temperature of about -150℃ the propane mass flow should be about 1.5 kg/s (3.05 l/s). This is found by a simple simulation in

Aspen Hysys and for an inlet temperature of about 0℃. Propane pressure will be high enough to ensure liquid state at all times (8 bar).

The heat exchanger shell side volume is 11.612 litres.

The mass flow of glycol will set to the same as propane. The heat flow and temperatures can thus be compared. It is desirable to investigate the conditions for different glycol/water mixtures. Therefore the experiments will be carried out for three different glycol-water solutions: 40w%, 50w% and 60w%.

The water (水) loop

The water mass flow will be set to serve the IF heat duty according to its needs. Hysys investigations show that the water mass flow should generally be in the same order and slightly higher than the mass flow of propane. The suggested water flow is 2 kg/s (2 l/s). However, the water flow rate will be determined in the preliminary (test) experiments in which a reasonable propane temperature will be reached. The same mass flow will be used for ethylene glycol.

It is desirable to investigate the impact of different water temperatures on the system. IF regasification allows the use of colder water than normal open rack vaporizers; the minimum water temperature can be as low as 1℃, while ORVs require minimum 5℃. Therefore the water temperature should be supplied at 3 different temperatures: 1℃, 5℃ and 15℃. Each water temperature will ideally serve in 4 experiments, for propane and the 3 different glycol concentrations. Time is the determining factor.

A1.7 Equipment

All equipment and instruments are described below.

The water loop

1. The water tank volume
   $G_m = 0.53kg/s$, $V = 3m/s$, and the length of the entire experiment section is 20m.
   The time for one full water circulation is $t = \frac{L}{V} = \frac{20}{3} = 6.67s$. Taking into account resistance and other factors, the real flow time will be 100s, so the required mass of water is 53kg. The tank volume is thus 53 l. Considering that there is a evaporator in the refrigeration unit, the tank volume is chosen to be 100l.
2. Refrigeration unit
   The cooling capacity should be able to handle up to 70 kg of water to avoid strain on the refrigeration system. With 70 kg water and $T_{in} = 25℃$, $T_{out} = 7℃$ the required cooling

capacity is 1.463kW. At this value the refrigeration unit need 1 hour to cool the water to the target temperature.

3. Electric heating group
   It is assumed that the Δt of water after heat exchange with propane is 5K, so the maximum electric heating power needed is $Q_{\max} = G_m C_p \Delta t = 11kW$. The electric heating can adjust the power according to the change of temperature to ensure that the outlet temperature of water is correct.
4. Technical requirements
   It is desirable to do experiments with water temperatures from 1℃to 20℃. The refrigeration unit and electric heating should be able to start and stop according to input from to temperature control device

Flow control valve and mass flowmeter

There are three kinds of control valves in the system: IF flow control valve, water flow control valve and LN2 flow control valve.

IF: $p_{\max} = 1MPa$, $t = -50 \sim 10^{\circ}C$, $G_m = 0.1 \sim 2kg/s$

The physical properties of propane: $\rho = 536.17kg/m^3$, $Gv = 0.524 \sim 5.24m^3/h$

Purity requirement of propane: 99%; diameter: 15-16mm; pressure:1.6MPa; minimum temperature: -20℃, valves are welded in the pipeline system.

Water: $p = 0.1MPa$, $t = 25 \sim 7℃$, $G_m = 0.53kg/s$;

The physical properties of water: $\rho = 1000kg/m^3$, $Gv = 1.908m^3/h$;

Diameter: 15-16mm; pressure: ordinary pressure; temperature: 7-25℃; valves also welded in pipeline system.

IF delivery pump and water delivery pump.

IF: $p_{\max} = 1MPa$, $t = -50 \sim 10$, $G_m = 0.1 \sim 2kg/s$

The pump model is a liquefied petroleum gas delivery pump of model YQB5-5, with rated flow $5m^3/h$

Water: $G_m = 0.53kg/s$, maximum mass flux $G_{\max} = 2kg/s$. The rated flow of water is $7.2m^3/h$ and the head of delivery is $H = \frac{p}{\rho g} = 11m$. The pump is a low flow rate, high head pump, with flow allowance of 10%.

Thermocouples

All temperatures are measured by thermocouples; propane temperatures, water temperatures and inner tube surface temperatures. The thermocouples are of the type PT-100, purchased from the Chinese Academy of Sciences.

Pressure transmitter

The pressure is measured at the inlets and outlets of propane in the heat exchangers. The maximum pressure of propane is $p = 1Mpa$ and the minimum pressure is $p = 0.5Mpa$. 2 pressure transmitters has been purchased.

IF storage tanks

The length of the whole experiment system is 10m and the flow velocity of propane is 0.1m/s. The time required for one loop of IF flow circulation is 100s. IF will flow at 5m³/h and the storage tank volume needed is 138.8L. To avoid approaching the limit the tank is chosen to be 200l.

Appendix 2: Laboratory log

Preliminary work

- The previous system, used by Ji Xin and Chen Shuangshuang, is still present in the lab. It will be simplified and changed.
- Isolation on the old system has been removed carefully. It will be reused in the new system
- Other parts, sensors etc. are disconnected.
- The two heat exchangers will be exchanged with new ones. The two new heat exchangers, built as one steel pipe inside another, are built and welded by Mr. Liu.

28.04.2015

- The new heat exchangers are installed in the modified system. Connections are tightened with new seals. The system is somewhat simplified as there is no need for phase-changing intermediate fluid in the future experiments.
- The holes that were bored for the thermocouple sensors probed to be too tight. The holes have been re-threaded.
- The thermocouple sensors, 18 in total, have been installed. Each heat exchanger have 5 sensors in the shell side flow region and one in each inlet and outlet. Each sensor was installed with a new rubber seal.
- The two pressure sensors are the only components missing. When they arrive the project will continue to testing for leakage.

11.05.2015

- The pressure sensors finally arrived and were installed. The leakage testing will commence tomorrow.

12.05.2015

- Leakage testing commenced.
    1. Test one: All connections and sensors were layered with soap bubbles and system was filled with nitrogen at 2 bar. One connection was found to lack a seal. A seal was installed and no more bubbles were produced.
    2. Test two: Nitrogen was filled into the system through a fill-in valve. The system pressure was increased to about 8 bar in 3 steps. Pressure was monitored. The

pressure did not drop throughout this day and the monitoring will continue through the night.

- A problem was encountered when connecting the pressure sensors to the electric monitoring equipment. Wan Xingcheng misread the instructions and connected the monitor to a 240 V outlet instead of a 24 V. The monitor suffered damage and cannot be used. The sensor itself was unharmed and a new monitor was connected successfully.
- Work on preparing the thermocouple sensors for connection was started. The sensors are of the 4-wire type. However the signal processing equipment does not have enough slots. Therefore the 4 wires of each sensor has to be combined to 2 wires. The work was carried out by testing the resistance difference between the wires with a multimeter. 2 wires without resistance difference can be combined to one wire, while wires with a resistance difference must be separated. The 2 combined wires were soldered to extension wires, tagged with serial number and taped to the heat exchanger body. The work was time-consuming and not finished.

13.05.2015

- The pressure has dropped by about 30 kPa overnight, from 0.860 MPa to 0.833 MPa. A small leakage was detected at the fill-in valve. The connection was plugged and the pressure is monitored further.
- Thermocouple sensor wire combining and extension work was completed.

14.05.2015

- The system pressure has decreased less than 10 kPa overnight and the system leakage is therefore deemed insignificant. No further work conducted today.

15.05.2015

- Started isolating all pipes. All pipes are to be isolated with a 10 mm thick isolation material and a rubber tape.

19.05.2015

- Isolation work completed. Temperature sensors connected to the signal processing device, a Keithley 2701 multimeter.

20.05.2015

- The nitrogen loop flowmeter was installed. All sensors and valves are now installed, though only the temperature sensors are connected. Pressure will be monitored on separate monitors.
- The computer was setup and connected to the processing device. Some problems with the connection to the processing device were encountered. These problems will be further investigated tomorrow.

21.05.2015

- The work on the computer and monitoring system was continued. No breakthroughs yet

25.05.2015

- A pressure drop has been identified during the weekend. The leakage was found at the connection of the pressure sensor at the inlet of the propane – water heat exchanger. The connection was not fastened tightly, this was remedied.

27.05.2015

- The work on the thermocouple sensors has been completed. Connectivity problems between the Keithley multimeter and the computer was solved by re-installing the relevant drivers and modify ExelLink, which is used to record the data.
- The sensors were found to report a too high temperature. The system has now been pressurized by nitrogen at about 8 bar for several days. The temperature should correspond to the room temperature, as measured by a mercury-in-glass thermometer (accuracy of thermometer is 0.1 degrees). The following were found:
    - The extension wires produce a relatively high resistance. The resistance were found to be 0.49 ohm per meter. The resistance is deduced from the recorded resistance according to the length of each wire.
    - Every sensor has a slightly different relationship between resistance and temperature. This relationship is assumed to be linear (deviations from linearity of maximum 0.2 ohm are observed). A linear function ($y = ax + b$) is found by using regression on the data points that are supplied with each sensor in a pamphlet. Thereafter the resistance is converted to temperature.
    - The sensor inaccuracy is 0.1 K
- After converting the resistance to temperature there is still an off—put on some of the sensors. Modifications were done in excel to add or subtract resistance until all sensors

displayed the same temperature +- 0.05 K. This process was repeated several times, until the sensors all gave a repeatable temperature reading equal to the recorded room temperature +- 0.3 K. This calibration process was only conducted at times with stable ambient temperature (afternoon, stable weather).

- The flow meters of water and IF was connected to the Keithley multimeter. They both had a reading of 0.3918 V for 0 flow.

28.05.2015

- Flow meter readings were transformed so they display the flow in cubic meters per hour. The relationship is linear and the conversion factors can be found in the excel raw data sheet.
- The calibration of the thermocouple sensors was controlled for errors. They stay within the previously found error limits.

29.05.2015

- System de-pressurized and the last pressure sensor was installed and calibrated.

01.06.2015

- Propane experiment to be carried out today. Some discussion and first-time preparation was carried out in the morning, such as positioning and connecting nitrogen and propane tanks to the system. The rest of the experiment will follow the procedures listed in appendix 1. Any deviations or problems will be written here
- Upon introducing nitrogen to the system a leakage was discovered at the nitrogen outlet. Note that only the IF loop was pressurized during the pressure testing. The seal was checked and the connection tightened. No leakage detected in the second trial.
- The heat in-leak of the nitrogen pipeline from the tank (stored outside) to the system is very large. The mass flow of nitrogen needs to be increased to reach a low inlet temperature. The nitrogen will be gaseous. The pipes from the nitrogen tank to the inlet of the nitrogen heat exchanger was re-insulated, as the old insulation was poor.
- The flow meters of water and propane are not working. Investigation commenced and will continue tomorrow.

02.06.2015

- The water flowmeter was disassembled. Rust and dirt was blocking the pipe and measuring wheel in the flow section. This was cleaned and the flowmeter value equal the value of the water pump. The flowmeter is now operational.

- Unable to repair the propane flowmeter. A new one has been ordered and will hopefully arrive quickly. No further work can be done until it arrives

05.06.2015

- The propane flowmeter will arrive Saturday. Experiments will continue Monday

08.06.2015

- Propane flow meter installed successfully and is working. Commencing experiments
- Some limitations to the experiment setup were found:
    - It is difficult to control the nitrogen flowrate. The valve on the nitrogen tank is the controlling unit, and obtaining the same flowrate for each experiment after closing and re-opening the valve will prove troublesome. However, the nitrogen temperature drop across the heat exchanger is small and as long as the nitrogen inlet temperature is about 80 K the impact of mass flow change will be small and negligible.
    - The initial temperature of propane was similar to ambient conditions, about 297 K. The experiments require cooling of the propane until it reach a stable temperature at some level between water and nitrogen, which require a long time. At least several hours will be needed between each water temperature setting (see exp procedure in appendix 1).
- Several test experiments were conducted. The nitrogen flowrate was kept constant and in the range of 10-25 m^3/h and nitrogen was flowing almost constantly for 11 hours. The propane temperature was lowered to stable temperatures in between 10 and 20 degrees. Refer to the data sheets for details (appendix 3).
- The nitrogen flowmeter output is fluctuating, sometimes by as much as 50 m^3/h, even though the valve is untouched and in the same position.

09.06.2015

- Main propane experiments are conducted
    - First experiment for water temperature at 293 K. The propane temperature has not increased above 293 K throughout the night and is thus more suited for experiments than yesterday.
    - Stable, unchanging temperatures reached fairly quick, after about 2 hours of running. Changed water temperature to 288 K.
- Successfully conducted experiments for water temperatures at 20, 15 and 10 degrees celcius.

10.06.2015

- Propane experiments are completed. No further lab work to be conducted today. The ethylene glycol experiments will commence tomorrow.

11.06.2015

- Propane is vented out of the tank to air. This required several hours
- Pumped the glycol-water mixture by hand pump into the IF tank.
- Apparently the tank temperature was still extremely low. Danger of glycol freezing. The freezing point of the glycol-water mix is interpolated from tables to -33.330°C
- The pump appear to be broken. It cannot pump the fluid and makes disturbing noises. It may have been frozen.

12.06.2015

- Bought new pump, a water pump (2.2 kW, Kaiyuan pumps model KYWR40-160). It fits the required specifications.
- The glycol-water mix is still cold. A temperature sensor was installed upstream of the pump on the outside of the pump. The temperature is deemed too cold to attempt a full-scale experiment

13.06.2015

- All propane is now vented to the air. Removed almost all of the glycol-water mix from the tank by pumping it into the blue barrel drum, which it was delivered in.
- Attempted running the experiment from the barrel drum. The pump works just fine, but the mixture is heated by the ambient conditions, and it is not possible to reduce the temperature.
- A large amount of oil, grease and other unwanted contaminants can be seen in the barrel drum after the glycol-water was removed from the system. As the pipes and heat exchangers were new and clean prior to the experiments, the contaminants most likely come from the tank and the pump. The contaminants increase the chance of fouling and may have contributed to the old pump failing.
- Pumped the glycol-water back into the adiabatic IF tank. The temperature can now be seen to drop slowly. Efforts were made to leave the contaminants (which largely floated on top of the liquid) in the barrel drum.

15.06.2015

- Experiments concluded.

Appendix 3: Experimental results

The following files provide the experiment results as excel data sheets. If you are reading the document non-electronically or for any other reason the links do not work, please refer to NTNU or SJTU to obtain access to the results.


Experiment 3 C3 20 degrees.xls


Experiment 5 C3 10 degrees.xls


Experiment 4 C3 15 degrees.xls


Experiment 7 MEG 20 degrees.xls